



5-1999

**An evaluation of absorption spectroscopy to monitor
YBa₂Cu₃O_{7-x} precursors for metal organics chemical vapor
deposition processing**

Matthew Edward Thomas

Follow this and additional works at: https://trace.tennessee.edu/utk_gradthes

Recommended Citation

Thomas, Matthew Edward, "An evaluation of absorption spectroscopy to monitor YBa₂Cu₃O_{7-x} precursors for metal organics chemical vapor deposition processing. " Master's Thesis, University of Tennessee, 1999.

https://trace.tennessee.edu/utk_gradthes/10036

This Thesis is brought to you for free and open access by the Graduate School at TRACE: Tennessee Research and Creative Exchange. It has been accepted for inclusion in Masters Theses by an authorized administrator of TRACE: Tennessee Research and Creative Exchange. For more information, please contact trace@utk.edu.

To the Graduate Council:

I am submitting herewith a thesis written by Matthew Edward Thomas entitled "An evaluation of absorption spectroscopy to monitor $\text{YBa}_2\text{Cu}_3\text{O}_{7-x}$ precursors for metal organics chemical vapor deposition processing." I have examined the final electronic copy of this thesis for form and content and recommend that it be accepted in partial fulfillment of the requirements for the degree of Master of Science, with a major in Engineering Science.

Thomas V. Giel, Major Professor

We have read this thesis and recommend its acceptance:

Atul Sheth, Roy Schulz, Brad Winkleman

Accepted for the Council:

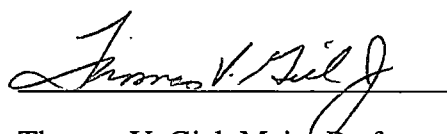
Carolyn R. Hodges

Vice Provost and Dean of the Graduate School

(Original signatures are on file with official student records.)


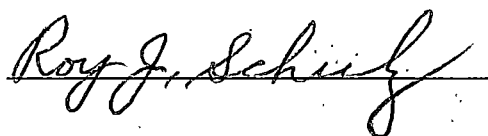
To the Graduate Council:

I am submitting herewith a thesis written by Matthew Edward Thomas entitled "An Evaluation of Absorption Spectroscopy to Monitor $\text{YBa}_2\text{Cu}_3\text{O}_{7-x}$ Precursors for Metal Organics Chemical Vapor Deposition Processing." I have examined the final copy of this thesis for form and content and recommend that it be accepted in partial fulfillment of the requirements for the degree of Master of Science, with a major in Engineering Science.



Thomas V. Giel, Major Professor

We have read this thesis
and recommend its acceptance:



Accepted for the Council:



Associate Vice Chancellor
and Dean of the Graduate School

**AN EVALUATION OF ABSORPTION SPECTROSCOPY TO
MONITOR $\text{YBa}_2\text{Cu}_3\text{O}_{7-x}$ PRECURSORS FOR METAL ORGANICS
CHEMICAL VAPOR DEPOSITION PROCESSING**

A Thesis
Presented for the
Master of Science
Degree
The University of Tennessee, Knoxville

Matthew Edward Thomas
May 1999

DEDICATION

This thesis is dedicated to my Lord and Savior, Jesus Christ. I also dedicate this thesis to my parents, Martin and Helen Thomas. Thank you for your consistent, Christ-centered example, prayers, unconditional love, support, and encouragement.

“But those who hope in the LORD will renew their strength. They will soar on wings like eagles; they will run and not grow weary, they will walk and not be faint.”

Isaiah 40:31 (NIV)

ACKNOWLEDGMENTS

I would like to express my sincere appreciation to the many individuals who helped make this work possible. Dr. Thomas Giel and Dr. Brad Winkleman have served as the supervisors for this research effort. Without their guidance, support, and assistance this thesis could not have been completed. Additionally, I would like to express a deep appreciation to Dr. Thomas Giel for his willingness to serve as my thesis advisor and committee chairman. Special thanks is also extended to Dr. Atul Sheth, Dr. Roy Schulz, and Dr. Brad Winkleman for serving as committee members.

I would also like to thank Mr. Wes McMinn for his valuable contributions to the design and development of the experimental apparatus. Lastly, I would like to thank the University of Tennessee Space Institute for providing me with a graduate research assistantship.

ABSTRACT

Absorption spectroscopy was evaluated as a technique to monitor the metal organics chemical vapor deposition (MOCVD) process for forming $\text{YBa}_2\text{Cu}_3\text{O}_{7-x}$ superconducting coated conductors.

Specifically, this study analyzed the feasibility of using absorption spectroscopy to monitor the MOCVD supply vapor concentrations of the organic ligand 2,2,6,6-tetramethyl-3,5-heptanedionate (TMHD) metal chelates of barium, copper, and yttrium. $\text{Ba}(\text{TMHD})_2$, $\text{Cu}(\text{TMHD})_2$, and $\text{Y}(\text{TMHD})_3$ compounds have successfully been vaporized in the MOCVD processing technique to form high temperature superconducting "coated conductors," a promising technology for wire fabrication.

The absorption study of the barium, copper, and yttrium (TMHD) precursors was conducted in the ultraviolet wavelength region from 200nm to 400nm. To simulate the MOCVD precursor flows the $\text{Ba}(\text{TMHD})_2$, $\text{Cu}(\text{TMHD})_2$, and $\text{Y}(\text{TMHD})_3$ complexes were vaporized at vacuum pressures of (0.03-10)Torr. Spectral absorption scans of each precursor were conducted to examine potential measurement wavelengths for determining vapor concentrations of each precursor via Beer's law.

The experimental results show that under vacuum conditions the barium, copper, and yttrium (TMHD) precursors begin to vaporize between 90°C and 135°C, which are considerably lower vaporization temperatures than atmospheric thermal gravimetric analyses indicate. Additionally, complete vaporization of the copper and yttrium (TMHD) precursors occurred during rapid heating at temperatures between 145°C and 195°C and after heating at constant temperatures between 90°C and 125°C for approximately one hour, whereas the $\text{Ba}(\text{TMHD})_2$ precursor did not completely vaporize. At constant temperatures, near constant vaporization levels for each precursor were observed for extended periods of time. Detailed spectroscopic scans at stable vaporization conditions were conducted.

TABLE OF CONTENTS

CHAPTER	PAGE
I. INTRODUCTION	1
II. BACKGROUND	7
MOCVD Technique	7
Absorption Spectroscopy	9
Spectroscopic Studies of MOCVD Precursors	16
III. EXPERIMENTAL ANALYSIS	26
Experimental Apparatus	26
Experimental Calibration	31
Experimental Precursor Absorption Procedures	40
Sources of Error	47
IV. EXPERIMENTAL RESULTS	52
Cu(TMHD) ₂ Absorption Experimental Results	52
Y(TMHD) ₃ Absorption Experimental Results	61
Ba(TMHD) ₂ Absorption Experimental Results	62
Analysis of Results	69
V. CONCLUSIONS AND RECOMMENDATIONS	79
REFERENCES	82
VITA	85

LIST OF TABLES

TABLE	PAGE
1. Beer-Lambert Law Nomenclature [12]	17
2. Precursor Precision Uncertainties	50
3. Comparison of Measured Absorption Peak Wavelengths with Reference [15]	72
4. Precursor Extinction Coefficient Calculations	74
5. Sensitivities of Cu(TMHD)_2 , Y(TMHD)_3 , and Ba(TMHD)_2	75
6. Precursor Vapor Pressure Calculations	77

LIST OF FIGURES

FIGURE	PAGE
1. MOCVD Superconductor Coating Process [5]	10
2. UV Reference Spectra of Cu(TMHD)_2 and Y(TMHD)_3 [6]	19
3. Reference Precursor Absorption Spectra [15]	22
4. Cu(DPM)_2 Reference Spectra [17]	24
5. Precursor Structure Diagrams [15]	25
6. Experimental Setup	27
7. Absorption Chamber Dimensions	29
8. Spectrometer Calibration of 253.652nm Mercury (Hg) Spectral Line	32
9. Spectrometer Calibration of 404.656nm Mercury (Hg) Spectral Line	33
10. Spectrometer Calibration of 435.833nm Mercury (Hg) Spectral Line	34
11. Spectrometer Calibration Data	35
12. Absorption of NO Gas at 0.05Torr, 0.10Torr, and 0.15Torr	37
13. Absorbance Ratios of NO Gas	38
14. Pressure Gauge Calibration Data	39
15. Capacitance Manometer Calibration Data	41
16. Y(TMHD)_3 Transmitted Intensity as a Function of Temperature	44
17. Y(TMHD)_3 Transmitted Intensity as a Function of Time	45
18. Cu(TMHD)_2 Thermogravimetric Analysis [18]	53
19. Y(TMHD)_3 Thermogravimetric Analysis [18]	54
20. Ba(TMHD)_2 Thermogravimetric Analysis [18]	55
21. Cu(TMHD)_2 Absorption Scan	57
22. Cu(TMHD)_2 Absorption	58
23. Cu(TMHD)_2 Absorption (200-220)nm Region	59
24. Cu(TMHD)_2 Absorption (220-260)nm Region	60

25. Y(TMHD) ₃ Absorption Scan	63
26. Y(TMHD) ₃ Absorption	64
27. Ba(TMHD) ₂ Absorption Scan: Trial 1	65
28. Ba(TMHD) ₂ Absorption: Trial 1	66
29. Ba(TMHD) ₂ Absorption Scan: Trial 2	68
30. Ba(TMHD) ₂ Absorption: Trial 2	70
31. Transmission Check of Sapphire Windows	71
32. Detailed Precursor Baseline Scans	78

NOMENCLATURE

A	Absorbance
a	Absorptivity or extinction coefficient
$Ba(TMHD)_2$	Barium precursor
b	Fixed absorption pathlength
$Cu(TMHD)_2$	Copper precursor
C	Concentration of the absorbing material
ΔC	Concentration uncertainty
ΔC_b	Concentration bias uncertainty
ΔC_p	Concentration precision uncertainty
C_m	Molar concentration of the absorbing material
c	Speed of light
DPM	Dipivaloylmethanate
e	Charge of the electron
f	Oscillator strength
I	Absorption scan intensity
I_0	Baseline scan intensity
J_c	Critical current density
K_v	Absorption coefficient
k_λ	Wavelength dependent proportionality constant
k'_λ	$-(k_\lambda b)/C$, dimensional factor utilized in derivation of Beer's law
k''_λ	$-k_\lambda/C$, dimensional factor utilized in derivation of Beer's law
l	Absorption pathlength
M	Precursor molecular weight

m	Precursor vapor mass
m_e	Electron mass
n	Number of moles
N_ν	Number of atoms per unit of volume (cm^3) which absorb radiant energy between ν and $\nu + d\nu$
P	Pressure
R	Ideal gas law constant
T	Temperature
T_c	Transition Temperature
τ	Transmission
TMHD	2,2,6,6-tetramethyl-3,5-heptanedionate
V	Absorption chamber volume
$Y(\text{TMHD})_3$	Yttrium precursor
ν	Frequency
ϵ	Molar absorptivity (molar extinction coefficient)
λ	Wavelength

Abbreviations

CVD	Chemical Vapor Deposition
HTSC	High Temperature Superconductors (Superconducting)
IBAD	Ion-Beam Assisted Deposition
IR	Infrared
LANL	Los Alamos National Laboratory
MOCVD	Metal Organics Chemical Vapor Deposition
MOD	Metal Organics Decomposition
MRI	Magnetic Resonance Imaging
NO	Nitrogen Oxide

OPIT	Oxide-Powder-In-Tube
ORNL	Oak Ridge National Laboratory
RABiTS	Rolling Assisted, Bi-Axially Textured Substrate
UTSI	University of Tennessee Space Institute
UV	Ultraviolet
YBCO	$\text{YBa}_2\text{Cu}_3\text{O}_{7-x}$
YSZ	Yttria-Stabilized Zirconia

CHAPTER I

INTRODUCTION

Superconductivity is a phenomenon that occurs at very low temperatures. Every superconductor has a transition temperature T_c below which it has essentially zero direct current resistance for currents less than a critical current density, J_c . As the temperature drops below T_c , the J_c value increases. In the superconducting state, the material has no electrical resistance. Additionally, in the superconducting state the material exhibits perfect diamagnetism, and it repels any applied magnetic field. In the normal state the material does have resistance, and the current accompanies the development of heat and the dissipation of energy [1].

In 1908 H. Kamerlingh Onnes of the University of Leyden in Holland developed a procedure to liquefy helium. Helium liquefaction occurs at 4.2 Kelvin (K) (-268.8°C). To bring about this liquefaction, helium gas is compressed to a smaller volume. This compression causes the temperature of the helium gas to rise. The warmed compressed gas is then passed through a pipe surrounded by a colder fluid. This causes heat to be removed from the gas and transferred to the fluid. The still compressed, cooler gas is now forced through a small hole beyond which it expands to lower pressure and temperature. This cool gas can be used to further cool compressed helium. These steps are repeated over and over again until the temperature of the compressed gas reaches 4.2K where it liquefies. This process that Onnes used to liquefy helium is still used today in modern refrigerators [1].

Having successfully liquefied helium, Onnes now had the ability to cool other materials to 4.2K by simply lowering them into a helium bath. Onnes then began to carry out experiments on materials immersed in liquid helium. These experiments had never been possible. One of the first of these, carried out in 1911, was to measure the electrical

resistance of solid mercury. The experimental measurement consisted of applying a voltage V across the mercury, recording the current I , and calculating the resistance R by dividing the voltage by the current, ($R = V/I$). While the mercury was at 4.3K, Onnes noticed that if he turned off the voltage, the current stopped, as expected. He also noticed that if he turned off the voltage below 4.2K, the current continued. In fact, the current continues without losses for months and even years because the resistance of the material is zero [1]. With this observation, the study of superconductivity was born.

In Onnes' time superconductors were simple metals like mercury, lead, and bismuth. These elements become superconductors only at the very low temperatures of liquid helium. In the next 75 years, great strides were made in the understanding of how superconductors worked. During that time, various alloys were found that were superconductors at somewhat higher temperatures. Unfortunately, none of these alloy superconductors worked at temperatures much higher than 23K. Thus, liquid helium remained the only convenient refrigerant that could be employed as a cooling medium with these superconductors [2].

For the next several decades, superconductors remained a scientific curiosity with few practical applications because the known superconductors lost this property at low current flows. Then in the 1960s a practical superconducting metal wire made of niobium and tin was developed. That wire, later made of a niobium and titanium alloy, became the basis for the first applications of superconductors with high J_c even in a substantial magnetic field [3].

The niobium and titanium alloy, still in use today, is among the materials called low-temperature superconductors. Low-temperature superconductors must be cooled to below 20K in order to become superconducting. They are now widely used in magnetic resonance imaging (MRI) machines and in the fields of high-energy physics and nuclear fusion. Additional commercial use has been limited largely by the high refrigeration costs

associated with liquid helium, which is needed to cool the materials to such low temperatures [3].

The hope for low-cost superconductivity was ignited by two significant discoveries in the 1980s. In 1986, two IBM scientists in Zurich, Switzerland, Alex Müller and Georg Bednorz, discovered a new class of superconductors. Unlike the low-temperature superconductors, which were metallic or semimetallic, these new compounds were ceramic and were superconducting up to 35K. Müller and Bednorz won a Nobel Prize for their discovery. Then in 1987, Paul Chu at the University of Houston took the discovery one step further and announced a compound that became superconducting at 94K. This discovery was particularly significant because this compound could be cooled with cheap and readily available liquid nitrogen. These new materials were dubbed high-temperature superconductors [3].

There are several advantages in using liquid nitrogen instead of liquid helium. The 77K temperature of liquid nitrogen is far easier to attain and maintain than the 4.2K of liquid helium. Liquid nitrogen also has a much greater capacity to keep things cold than does liquid helium. Most importantly, nitrogen constitutes 78% of the air we breathe, and compared to liquid helium for which there are only a few limited sources, it is much cheaper [2].

Today's high-temperature superconductors are moving out of the laboratory and into the marketplace. Bismuth-based compounds are being fashioned into superconducting wires and coils, which are essential to electric power uses. Thallium- and yttrium-based compounds are being formed into thin conducting films used in electronic devices. And, as superconductivity moves into the 21st century, products such as superconducting motors, generators, fault-current limiters, energy storage systems, and power cables promise to change forever the way electricity is generated, delivered, and used [3].

The discovery of superconductivity at temperatures above liquid nitrogen temperature continues to attract great interest because of its enormous potential commercial applications. The superconductor of choice for most wire applications is $\text{YBa}_2\text{Cu}_3\text{O}_{7-x}$ (YBCO). Much research on high temperature superconducting (HTSC) wire manufacturing concentrates on the YBCO compound because it has high J_c values and remains superconducting in high magnetic fields and because its T_c of (90-95)K is high enough for applications under liquid nitrogen [1]. However, research is needed on YBCO wire manufacturing because YBCO has good performance only if individual crystalline grains show a high degree of alignment. Fortunately, biaxially aligned YBCO thin and thick film strips have been grown on textured substrates. The resulting YBCO "coated conductors" carry more current than do superconducting compounds in the bismuth family and are better suited to high magnetic field applications. Coated conductors of YBCO have demonstrated critical currents exceeding one million amperes per square centimeter at 77 Kelvin, orders of magnitude above Oxide-Powder-In-Tube (OPIT) wire [4].

In the last few years, a major worldwide research effort has been devoted to the OPIT method to make high T_c superconducting wires and tapes. The OPIT method has been used to make superconducting wire using compounds in the bismuth family. However, the OPIT technique when applied to YBCO does not produce acceptable superconducting wires. Therefore, researchers trying to develop YBCO based superconductors have been attempting a number of physical and non-physical (chemical) deposition methods [5]. As of today, two different approaches for obtaining the textured substrates and subsequent YBCO coated conductors have been identified. These are: Los Alamos National Laboratory's (LANL) application of ion-beam assisted deposition called (IBAD), to obtain a textured YBCO coated conductor over a highly textured yttria-stabilized zirconia (YSZ) buffer on nickel alloy strips, and Oak Ridge National Laboratory's (ORNL) rolling assisted, bi-axially textured substrate option called RABiTS [5].

The following are some physical and non-physical deposition methods currently being studied to manufacture YBCO coated conductors [5]:

- Chemical Vapor Deposition (CVD)
 - * Metal Organics Chemical Vapor Deposition (MOCVD)
 - * Plasma or Photo-Assisted MOCVD
- Sol-Gel (Spin/Dip-Coating, Spraying, Painting)
- Metal Organics Decomposition (MOD)
- Electrodeposition
- Aerosol/Spray Pyrolysis

This research effort concentrates on control technology for the MOCVD technique to form high T_c superconducting YBCO thin films. MOCVD fabrication of high temperature superconductor films offers many advantages over alternate methods. However, one of its major weaknesses is associated with control of the gas phase delivery of the precursor materials. Precursors of choice to produce large scale YBCO thin films are the 2,2,6,6-tetramethyl-3,5-heptanedionate (TMHD) complexes of yttrium, barium, and copper. These complexes are also called dipivaloylmethanate (DPM) complexes. The physical properties of these materials make them candidates for use in MOCVD processing. They gasify at modestly elevated temperatures of (100-300)°C, but the barium derivative has limited volatility and is unstable at temperatures elevated above the atmospheric pressure vaporization temperature of 300°C [6].

To consistently produce high quality single phase YBCO by MOCVD, precise precursor delivery is required. Since one of the basic steps in MOCVD is precursor evaporation, chemical or physical changes in the precursor can affect evaporation rates and, therefore, film composition. The reason for the lack of suitable methods for the delivery of precise quantities of precursors is due to the varying physical characteristics and possibly

varying chemical characteristics of the precursors. These difficulties have led to both synthesis of alternate precursors and development of new precursor delivery techniques. Ultrasound measurement techniques have been used to monitor precursor delivery in MOCVD processing, but they provide little information on gas phase speciation [6].

At present, therefore, there is a need for a method to monitor and measure the controlled delivery of YBCO precursors for deposition in a MOCVD process. Gas phase spectroscopic absorption measurements are often used for species concentration monitoring and should be applicable to MOCVD precursors in gas phase. Hence, the purpose of this study was to evaluate the feasibility of using absorption spectroscopy to monitor the gas phase concentrations of the yttrium, barium, and copper (TMHD) YBCO precursors in their delivery system for MOCVD coated conductor processing.

CHAPTER II

BACKGROUND

MOCVD Technique

Before the discovery of high-temperature superconductivity in 1986, it was widely believed that the realization of superconductivity above 77K would provide many viable products for various applications. However, it is clear that turning this discovery into viable products is as challenging as was the discovery of the high-temperature superconductors. For coated conductor applications, metal organics chemical vapor deposition (MOCVD) can play a major role in the realization of high-temperature superconductor products. MOCVD has played a major role in the development of nonelectrotechnology related products due to high throughput, low-temperature deposition, sharp interface capabilities, and selective deposition with direct ion-, electron-, and photon-beam-controlled techniques. Selective deposition of superconducting and dielectric materials is of great importance in the realization of high-performance three-terminal switching devices. In addition, it is well documented that the critical current density of multi-crystal high-temperature superconductors are lower as compared to the textured coated conductors of the same material. Hence, MOCVD, in addition to well-established roles in the semiconductor and optoelectronics industry, can play a similar major role in the superconductivity industry because MOCVD holds promise for depositing superconducting coatings on substrates, since coated conductors are superior to other flexible superconducting materials [7].

MOCVD is a film deposition process in which growth is achieved by transporting individual components, by means of volatile organometallic sources, to a substrate heated to a temperature that decomposes the organometallic compounds. This releases the metals

on the substrate where they react to form the desired material if they arrive at the right stoichiometry. The advantages of MOCVD include its relative simplicity and controllability, leading to good adherence and reduced susceptibility to interfacial mixing and cross-contamination effects. In addition, it can produce a wide variety of materials at near-theoretical density, or controlled lower density. Reactions are irreversible, with no evidence of autodoping during epitaxial growth. This characteristic allows highly abrupt changes in doping and/or composition of epitaxial layers, with transitions within a few monolayers of growth. These unique features have made MOCVD the technique of choice for the deposition of ceramic and electronic materials and have led, in recent years, to extensive studies of its applicability to the growth of high temperature superconductors [8].

More importantly, MOCVD has many unique features which makes it especially attractive for the growth of high T_c superconductors for large-scale industrial applications, such as power transmission lines. These include the ability to provide high uniformity over a large area and high growth rates. MOCVD, in contrast to physical vapor deposition techniques, does not require a high vacuum environment and, accordingly, has the advantage of relative ease in scale-up to long lengths of tape. Also, it has the ability to coat substrates of complex shape and form, a feature which is limited only by the crystal orientation of the substrate when epitaxial films are desirable as with YBCO [8].

High quality YBCO coated conductors, with $T_c > 89\text{K}$ and $J_c (77\text{K}) > 10^6 \text{ A/cm}^2$ have been routinely deposited at substrate temperatures around 700°C by MOCVD. However, in order to fully develop this technology and realize its advantages, it will be necessary to understand and correlate the effects of process parameters (such as pressure, temperature, and reactant concentrations) with resultant film properties. Furthermore, an effort must be made to understand the fundamental chemistry associated with oxide-based MOCVD processes. Many of the growth parameters in MOCVD critically affect the structural and microstructural properties of the in-situ deposited films and, consequently,

the film's physical and electrical properties. A detailed picture of the relationships between these parameters and the film properties must be established. This is needed in order to precisely determine the conditions for the in-situ growth of HTSC thin films with the desired crystal structure and optimum superconducting properties [9]. Figure 1 illustrates the MOCVD processing technique for high temperature superconducting coated conductor wire fabrication.

Absorption Spectroscopy

Absorption spectroscopy is based on the phenomenon that matter absorbs electromagnetic radiation at frequencies characteristic of the absorbing species with a photon flux proportional to the number of species "particles" (atoms or molecules) absorbing the radiation. This matter when properly energized, may emit energy as electromagnetic radiation at the same frequencies characteristic of the absorption and with a photon flux proportional to the number of particles participating in radiation. Thus, the frequencies absorbed or radiated serve to identify the absorbing or radiating species, whereas the amount of radiation gives a measure of the quantity of the matter responsible for the absorption or emission. These two properties constitute the bases of, respectively, qualitative and quantitative analytical spectroscopy [10].

The first investigations of the nature of visible radiation are due to Newton, who used a glass prism to study the composition of the radiation emitted by the sun. His discovery of the visible spectrum with its seven colors was followed, almost 100 years later, by the discovery of the infrared region and Ritter's discovery of the ultraviolet region. During the first half of the eighteenth century, further investigations by Young, Wollaston, Fraunhofer, J. F. W. Herschel, Brewster, Wheatstone, Becquerel, Draper, Stokes, Helmholtz, Meyerstein, Crookes, Esselbach, Willigen, Müller, Foucault, and Boisbaudran constituted basic contributions to the field of spectroscopy. It was due solely to the genius

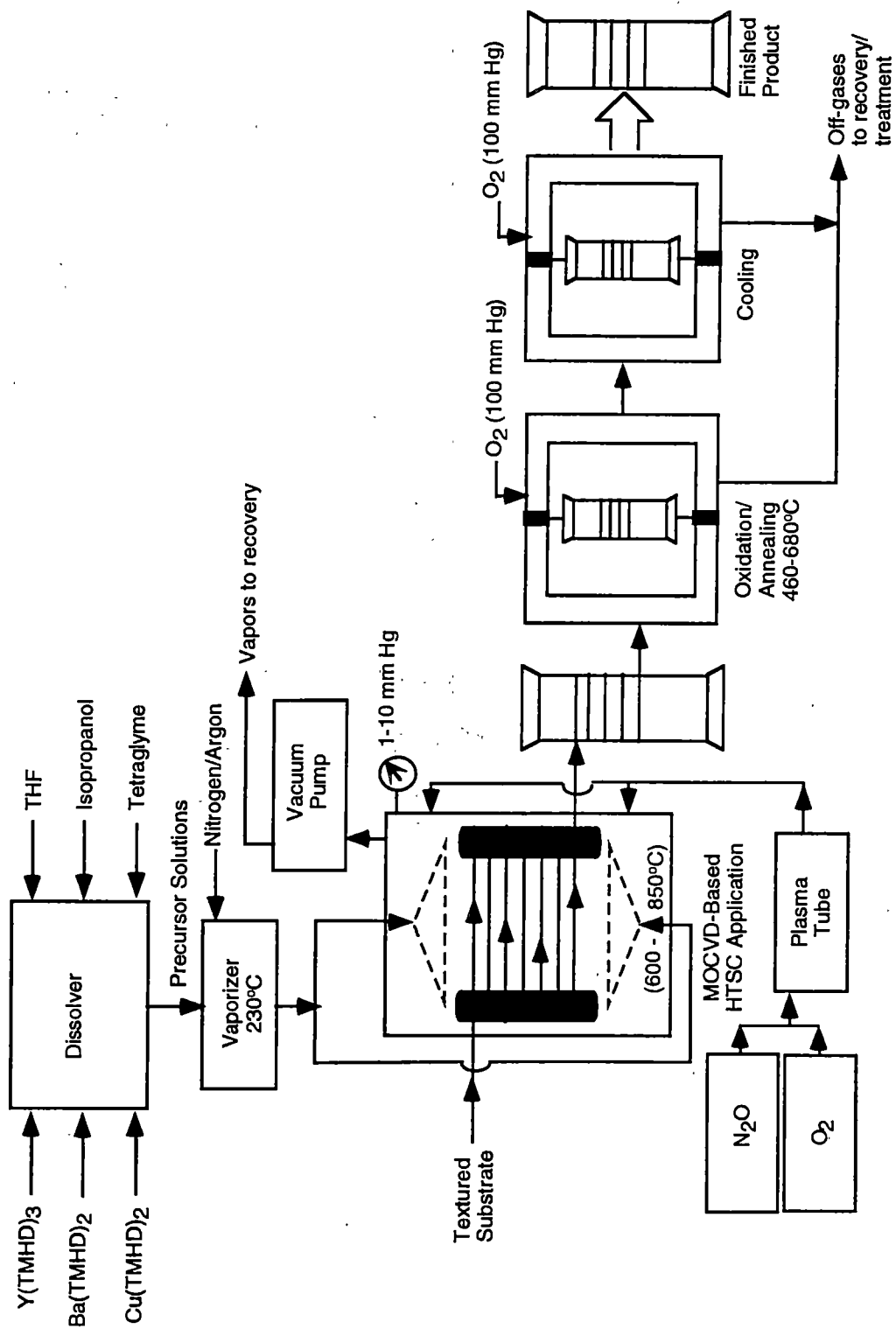


Figure 1. MOCVD Superconductor Coating Process [5].

of Kirchhoff and Bunsen, however, that a new method of research and measurement was created: analytical spectroscopy [10].

In numerous qualitative investigations they used the flame of the Bunsen burner as the excitation source. The instrument developed by these two scientists had all the major components found in modern spectrosopes: variable slit, collimating lens, prism, telescope for visual examination of the spectrum, and reference scale. With this powerful new research tool they established the basis of qualitative spectral analysis and elegantly demonstrated the method by the discovery of two previously unknown elements: rubidium and cesium. Using this method, Crookes in 1861 discovered thallium, and Reich and Richter discovered indium [10].

Atomic absorption and atomic absorption methods form a distinctive offshoot of spectroanalysis by flame methods. However, there are other means of producing absorption which may be used in a similar way for analysis, without the use of a flame. Hence, it seems wise to define the method in general terms, on the basis of the absorption process. Thus, this branch of analysis is usually called atomic absorption spectroscopy. This term, which was introduced by Walsh, denotes any analytical method in which an element is atomized in order to permit the observation, selection, and measurement of its electromagnetic radiation absorption spectrum [11]. It is applicable to molecules as well as atoms and, therefore, is better labeled absorption spectroscopy.

The method could be defined in general terms as an instrumental spectroanalytical method which is based on the measurement of the absorption produced, in a beam of radiation of suitable wavelength proceeding from an emitting source of constant intensity, by a medium composed of molecules of the species to be determined. Under these conditions, the amount of absorption increases with the concentration of molecules in the absorbing medium, and thus with the concentration of the species in the sample gas or solution used in producing the absorbing medium. If the sample is in gas, liquid, or solid

form, the absorption measured will increase with the concentration of the absorbing species in the sample, whether it be in its original condition or subjected to pretreatment [11].

Atomic vapors at moderate temperatures and ordinary pressures have absorption spectra consisting of sharp lines which lie within a range of wavelength, from 1800 to 9000 Å, convenient for selection with monochromators and spectrophotometers, and which are narrow enough to provide excellent specificity. To achieve the highest performance in atomic absorption measurements, the absorption must be measured at the wavelength corresponding to the peak of the absorption line, or within a rather narrow wavelength range very close to the peak. The inclusion of absorption flame photometry within the general method of absorption spectroscopy is due to the fact that the flame is used as a carrier of the absorbing medium formed of atoms. The flame is an effective means for producing and maintaining a suitable concentration of atoms, and the first experimental steps in this field were generally made with the aid of flames. Nevertheless, any procedure whose basis can be covered by the above definition may be considered a true method of absorption spectroscopy. Those procedures that use discrete emitters and flames to obtain atomic populations constitute only one of many possible cases falling under that definition [11].

In absorption flame photometry, a sample in liquid form is sprayed into an appropriate flame, and the analyte or analytes present are atomized. The analytes are determined by measuring the absorption of a beam of light passing through the flame. Each determination is made at the wavelength at which each analyte absorbs. The flame is placed between a constant-intensity source of light and a wavelength selector. Experimental readings are taken of the intensity of the light, as seen through the flame [11]. In absorption flame photometry, the radiation beam passes through a carrier flame containing the absorbing molecules, forming in this way an absorbing medium of a definite thickness. This absorbing medium acts as an absorbing cell [11].

Assuming that all the molecules considered in the absorbing medium are in a neutral form and in the ground state, and also assuming that there are no scattering effects, if a practically parallel beam of light of intensity $I_{0\nu}$ (at a frequency ν) traverses an absorbing pathlength b , the emerging beam will have an intensity I_ν given by

$$I_\nu = I_{0\nu} \exp(-K_\nu b) \quad (1)$$

The absorption coefficient K_ν varies with the frequency, because the absorption line has a finite width. It will also vary with all the factors that affect the width of the absorption line (temperature, pressure, nature of the molecules present in the absorbing medium, etc.) [11].

According to the classical theory of dispersion, the integrated atomic absorption

$$\int K_\nu d\nu \quad (2)$$

is given by

$$\int K_\nu d\nu = \frac{\pi e^2}{m_e c} N_\nu f \quad (3)$$

where

- N_ν = number of atoms per unit of volume (cm^3) which absorb radiant energy between ν and $\nu + d\nu$,
- f = oscillator strength,
- m_e = mass of the electron,
- e = charge of the electron,
- c = velocity of the light.

In a transition starting from the ground state, the integrated absorption is a linear function of the number of atoms, i.e. the concentration of absorbing atoms in the medium. It should be noted that neither the temperature nor the excitation potential appears in both

expressions. In equation 3 the value of the oscillator strength is included, which is the average number of electrons per atom which can be excited by the incident radiation [11].

The Bouguer-Lambert-Beer-Bernard law of equation 1, frequently called Beer's law, is fundamental in the consideration of the quantitative aspects of the absorption process in absorption spectroscopy [11]. The fractional amount of light absorbed and hence the fractional amount of light left for transmission are related to the thickness and absorbing species concentration of the sample. Beer's law may be derived as follows [12].

Let I be the intensity of a parallel beam of monochromatic light of wavelength λ , passing through a layer of thickness dl of an absorbing material. The change in intensity dI , is given by

$$dI = -k_{\lambda} I dl \quad (4)$$

where k_{λ} is a wavelength dependent proportionality constant. The negative sign is required because I becomes smaller as l becomes larger. The equation can be rearranged to give,

$$\frac{dI}{I} = -k_{\lambda} dl \quad (5)$$

This can be integrated between the limits I_0 and I , for l between 0 and b :

$$\begin{aligned} \int_{I_0}^I \frac{dI}{I} &= -k_{\lambda} \int_0^b dl \\ [\ln I]_{I_0}^I &= -k_{\lambda} [l]_0^b \\ \ln \frac{I}{I_0} &= -k_{\lambda} b \\ 2.303 \log_{10} \frac{I}{I_0} &= -k_{\lambda} b \\ \log_{10} \frac{I_0}{I} &= \frac{k_{\lambda} b}{2.303} \end{aligned} \quad (6)$$

If the species concentration C is the independent variable, as in Beer's law, and b is constant we can write equation 5 as

$$\frac{dI}{I} = k'_\lambda dC \quad (7)$$

where $k'_\lambda = -(k_\lambda b)/C$ results from manipulation of equation 5 and equation 6.

Integrating between the limits I_0 and I , and $C = 0$ and $C = C$ gives

$$\log_{10} \frac{I_0}{I} = -\frac{k'_\lambda C}{2.303} \quad (8)$$

Equations 6 and 8 for $\log_{10}(I_0/I)$ in b and in C can be combined to give,

$$\log_{10} \frac{I_0}{I} = -\frac{k''_\lambda b C}{2.303} \quad (9)$$

where $k''_\lambda = -k_\lambda/C$ is a dimensional factor resulting from manipulation of equations 6 and 8.

$\log_{10} I_0/I$ is called absorbance A , I/I_0 is called transmittance τ and $k''_\lambda/2.303$ is called molar absorptivity ϵ , when the concentration C_m is given in (g)(mol)(dm⁻³). Thus,

$$A = \epsilon b C \quad (10)$$

If the molecular weight of the sample material in solution is not known, the extinction value is used. This is defined as the absorbance, $A_{1cm}^{1\%}$ of a 1% with respect to volume solution measured in a $b = 1$ cm cell [12]. That is,

$$A_{1cm}^{1\%} = \frac{10\epsilon}{M} \quad (11)$$

Another way of representing Beer's law is

$$I = I_0 10^{-abC} \quad (12)$$

or

$$A = abC = \log I_0/I \quad (13)$$

In these equations I_0 is the intensity incident upon the first surface; I is the intensity transmitted through the thickness b ; C_m is the molar mass concentration of the absorbing material; and a is the absorptivity, which depends upon the frequency of the radiation as well as upon the nature of the substance. The absorbance A is more simply related to the concentration and absorptivity than is I or the ratio of I to I_0 and is therefore commonly employed in quantitative measurements [13]. Table 1 provides a description of Beer's law nomenclature.

Spectroscopic Studies of MOCVD Precursors

An extensive literature search found several publications involving spectroscopic studies of MOCVD precursors. Rappoli and DeSisto used ultraviolet spectroscopy to measure the gas phase concentration of 2,2,6,6-tetramethyl-3,5-heptanedionate (TMHD) complexes of Cu and Y in metal organics chemical vapor deposition bubbler effluent. The experimental measurements were made using a system consisting of a mass flow controller, temperature controlled bubbler, heated delivery lines, optical cell, spectrophotometer, cold trap, capacitance manometer, and vacuum pump. The objective of the experimentation was to examine the variability of TMHD complex delivery as a function of time and temperature by initiating a spectrophotometric study of $Y(TMHD)_3$ and $Cu(TMHD)_2$ precursors [6].

During the Rappoli and DeSisto isothermal studies, the bubbler, carrier lines, and optical cell were heated at 400, 405, 410K, respectively. The carrier lines and optical cell were thermostated at 10K above the maximum temperature of the bubbler during experiments in which gas phase concentration of the TMHD precursor was measured as a function of bubbler temperature. All measurements were made at 760Torr using 99.999% argon as a carrier gas at a flow rate of 50.0sccm. Heated carrier gas was passed through a 200cc dip-tube bubbler loaded with 5g of TMHD complex. Based upon prior studies, the

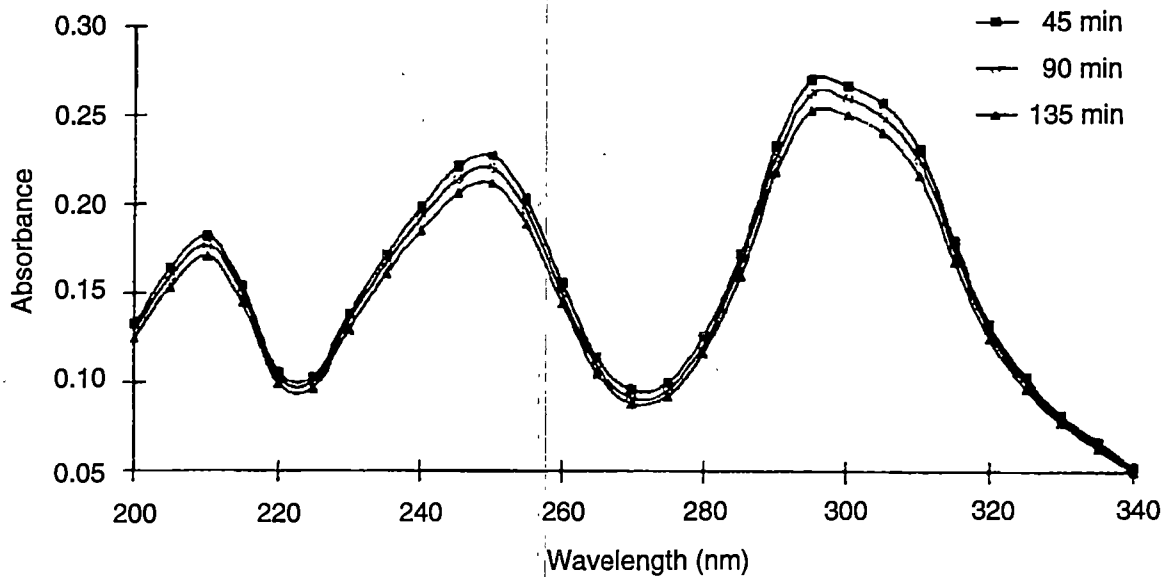
Table 1. Beer-Lambert Law Nomenclature [12].

Accepted Symbol	Meaning	Accepted Name	Alternate Symbol	Other Names
τ	I/I_0	Transmittance		Transmission
A	$\log I_0/I$	Absorbance	OD,D,E	Optical density, extinction
$A^{1\%}_{1cm}$	$10\epsilon/M$	Extinction Value	$E^{1\%}_{1cm}$	
a	$A/(bC)$	Absorptivity	k	Extinction coefficient, Absorbancy index
ϵ	$A/(bC_m)$ $C_m = \text{mol dm}^{-3}$	Molar absorptivity	a^M	Molar extinction coefficient
b	Path length of radiation through sample	Cell path	l or d	

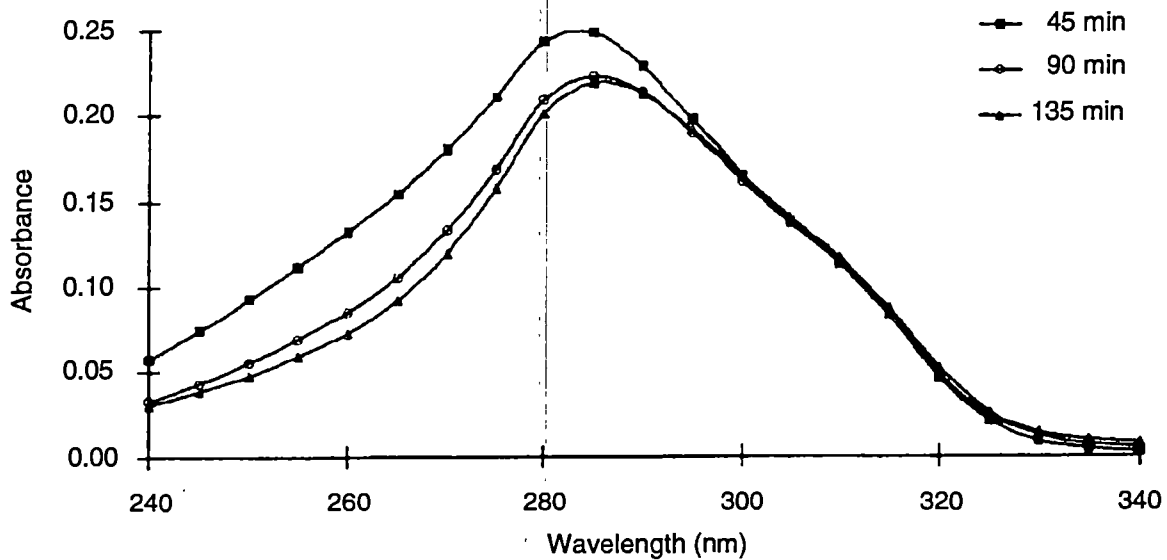
vapor pressure of the precursors at 400K were expected to be approximately 0.10 and 0.02Torr for Cu(TMHD)_2 and Y(TMHD)_3 , respectively. The effluent was carried to a 10cm path length high-temperature optical cell and finally through a cold trap. UV spectra were recorded using a Varian Cary 5E spectrophotometer. Gas phase spectra of Cu(TMHD)_2 and Y(TMHD)_3 were recorded between 200nm and 400nm with λ_{max} being observed at 297nm and 286nm, respectively. In isothermal experiments, spectra were recorded over a 4h period. Temperature dependent studies were initiated after a system purge of 2h [6].

The UV studies were designed to mimic conditions, except for pressure, of a typical MOCVD experiment. Initial experiments focused on the behavior of the Cu(TMHD)_2 and Y(TMHD)_3 since these precursors have high thermal stability. Figure 2 shows the results of gas phase UV spectra of Cu(TMHD)_2 recorded at 45min intervals. In Figure 2 the absorbance (absorption) change at 297nm is found to vary by 11% over 4h. Since flow rates were constant, then this change corresponds to a Cu(TMHD)_2 concentration change. Also, Figure 2 shows the changes observed for Y(TMHD)_3 . In the case of Y(TMHD)_3 , the absorbance (absorption) change at 286nm is found to drop by 14% over 4h. The concentration of Cu(TMHD)_2 and Y(TMHD)_3 in bubbler effluent begins to stabilize after 2h; however the concentration continues to decrease even after 8h of purging. Additionally, over a thirty day period the bubbler effluent concentration, after 2h of purging, was found to change by an average of 5% and 9% from day-to-day for Cu(TMHD)_2 and Y(TMHD)_3 , respectively [6].

In summary, two precursors, Cu(TMHD)_2 and Y(TMHD)_3 , typically used in YBCO film growth were characterized for long-term delivery stability. Variations in bubbler effluent concentration were observed over the course of a single study and from day-to-day. These variations are thought to be attributable to physical changes in the



(a) UV absorption spectra of Cu(TMHD)_2 recorded at 45min intervals.



(b) UV absorption spectra of Y(TMHD)_3 recorded at 45min intervals.

Figure 2. UV Reference Spectra of Cu(TMHD)_2 and Y(TMHD)_3 [6].

precursors, not decomposition. This shows the usefulness of UV spectroscopy for characterizing HTSC MOCVD precursor gas phase concentration in flow systems, as well as the need to monitor precursor concentrations. Obviously, UV spectroscopy could be used as a control monitor of precursor fluxes in a MOCVD precursor delivery system if it has appropriate sensitivity at typical MOCVD vacuum conditions [6].

Harima, Ohnishi, et al., conducted optical emission spectra experiments in the IR wavelength region of the β -diketonate chelates of Ba, Y, and Cu. Their experimentation consisted of vaporizing in an oven one of the source materials of $\text{Ba}(\text{DPM})_2$, $\text{Y}(\text{DPM})_3$, and $\text{Cu}(\text{DPM})_2$. The vapor was transported by argon to the glow-discharge region, and the IR optical emission from the vicinity of the grounded anode was observed by an optical multichannel analyzer. The oven temperature was raised from room temperature to 260°C for $\text{Ba}(\text{DPM})_2$, and to about 160°C for $\text{Y}(\text{DPM})_3$ and $\text{Cu}(\text{DPM})_2$. The nozzle portion was always kept a few degrees higher than the oven to avoid condensation of the vapor. These temperature ranges were chosen with reference to the reported values in previous precursor thermogravimetric experiments [14].

The results of their discharge experiments show that $\text{Y}(\text{DPM})_3$ and $\text{Cu}(\text{DPM})_2$ do not undergo thermal decomposition in the measured temperature range at wavelengths from 400nm to 650nm. Also, their experimental observations indicate that at above 220°C and in the 400nm to 650nm wavelength region, $\text{Ba}(\text{DPM})_2$ experiences enhancement of ionic emission intensity which can be associated with thermal decomposition. These researchers concluded that the strong excitation of barium is more probable in the decomposed forms since the barium ion can be exposed to electron collisions directly [14].

This group also conducted infrared spectra experiments on the $\text{Ba}(\text{DPM})_2$, $\text{Cu}(\text{DPM})_2$, and $\text{Y}(\text{DPM})_3$ precursors in the wavenumber region of 500cm^{-1} to 4000cm^{-1} . Similar to the discharge experimental results, the IR spectra show there are no appreciable changes for $\text{Cu}(\text{DPM})_2$ and $\text{Y}(\text{DPM})_3$ in the measured temperature range. This result may

be attributed to the difference of cross sections for decomposition and ionization by electron collisions. Additionally, the IR data show that some bands in Ba(DPM)_2 clearly become weak or disappear at higher temperatures [14].

The investigators of this research effort concluded that the discharge spectra of some β -diketonate chelates show variations reflecting the flux of source vapors and, possibly, their thermochemical changes such as decomposition that they have suffered during transport. If the correspondence between decomposition and the spectral pattern is well established, the discharge experiment could be used as a convenient diagnostic tool in actual deposition systems for monitoring the supply of delicate source gases such as Ba(DPM)_2 . These results will also be very helpful in proceeding with future in situ diagnostics [14].

A study on the stability of Y(DPM)_3 , Ba(DPM)_2 , and Cu(DPM)_2 with UV irradiation was performed by researchers at the Kyoto Institute of Technology. Figure 3 shows the results of their UV absorption experiments. The molar extinction coefficients of the tested materials of Y(DPM)_3 , Ba(DPM)_2 , and Cu(DPM)_2 were measured by a Shimadzu UV-visible spectrometer MPS-2000. The samples were dissolved in pure hexane with a concentration of $10^{-3} \sim 10^{-4}$ mol/l. They found that Beer's law was obeyed in all cases. This figure shows that Ba(DPM)_2 and Y(DPM)_3 commonly have a single peak at 270 ~ 280nm, although the Y(DPM)_3 peak has a weak shoulder on the red side. In contrast, the Cu(DPM)_2 spectrum is triply peaked in 200 ~ 300nm, and the largest one at about 300nm is doubly peaked [15].

Additionally, the Kyoto Institute of Technology researchers performed an IR spectral analysis of the Y(DPM)_3 , Ba(DPM)_2 , and Cu(DPM)_2 precursor complexes. The results showed that the chelate ring of Ba(DPM)_2 is most sensitively affected when irradiated in a 200 ~ 300nm region, and Y(DPM)_3 shows a similar, but much more modest reaction. On the contrary, Cu(DPM)_2 is very stable for all the light sources used. Such a

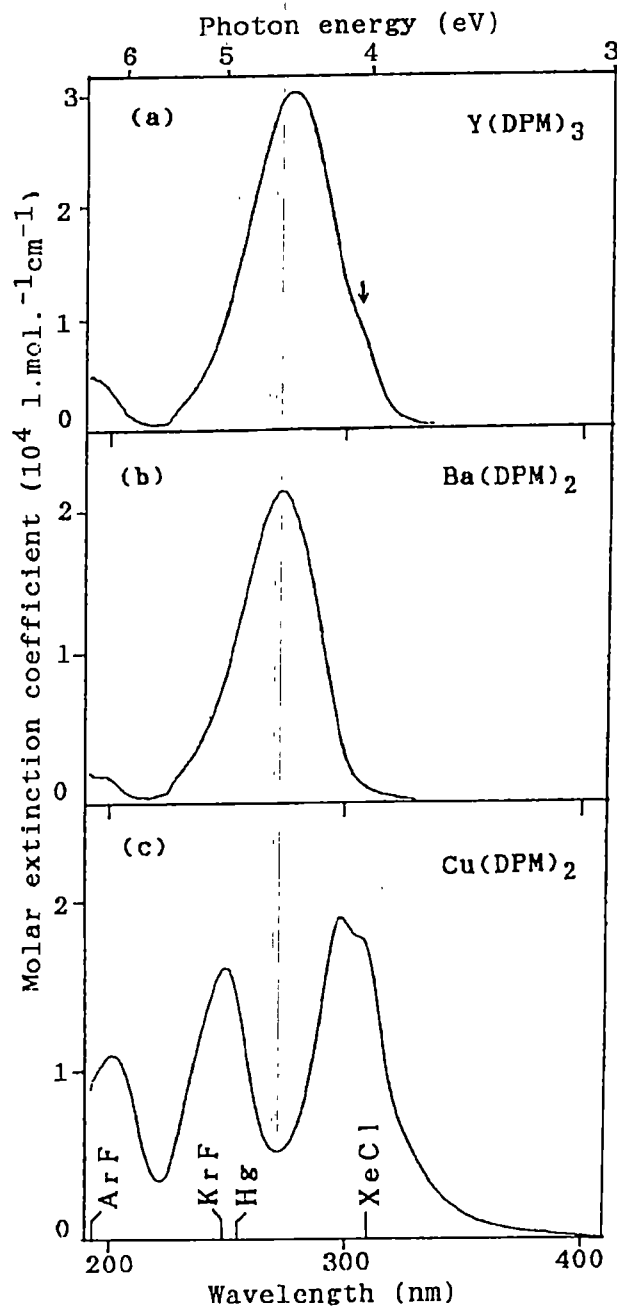


Figure 3. Reference Precursor Absorption Spectra [15].

difference of stability is deeply related to the metal-oxygen bonding nature of these chelates [15].

Thermal decomposition of Cu(DPM)_2 (bis(dipivaloylmethanate)copper (II)) in the gas phase was studied by in situ infrared spectroscopy combined with a MOCVD apparatus by Hanaoka, Ohnishi, Harima, and Tachibana of the Kyoto Institute of Technology. Decomposition was observed above 500°C of substrate temperature at a reactor pressure of 20Torr. Changes in the IR spectra when raising the substrate temperature showed that the C-C-C (carbon chain) bond in the chelate-ring structure or the carbon-tertiary-butyl bond is first broken in the decomposition process [16].

Lastly, Fackler, Cotton, and Barnum investigated the electronic spectra of Cu(DPM)_2 in cyclohexane in the ultraviolet to visible wavelength regions. The results of their work clearly indicate that higher absorption of the Cu(DPM)_2 complex occurs in the ultraviolet wavelength region than in the visible wavelength region [17]. These results are presented in Figure 4.

The TMHD and DPM precursors mentioned in this section are the same material. The structure of Ba(TMHD)_2 and Cu(TMHD)_2 are presented in Figure 5. Y(TMHD)_3 has a similar structure as Ba(TMHD)_2 and Cu(TMHD)_2 except the Y^{3+} ion is surrounded by six oxygen atoms of an octahedral configuration [15]. From the previously presented information, it is clear that absorption spectroscopy is a feasible diagnostic in monitoring the YBCO precursor concentrations, although the mentioned studies have not evaluated the precursor absorption bands under MOCVD pressure and temperature conditions.

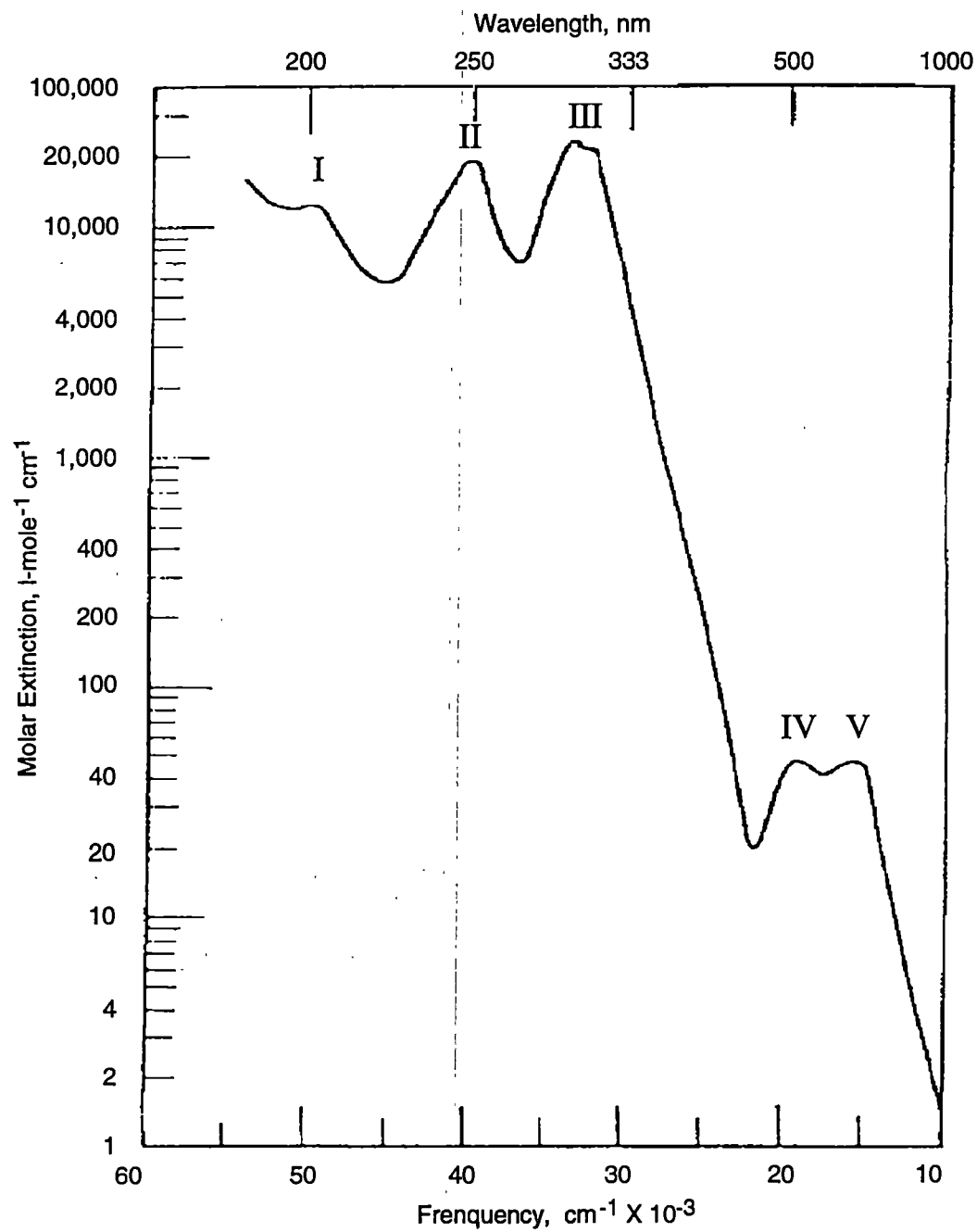
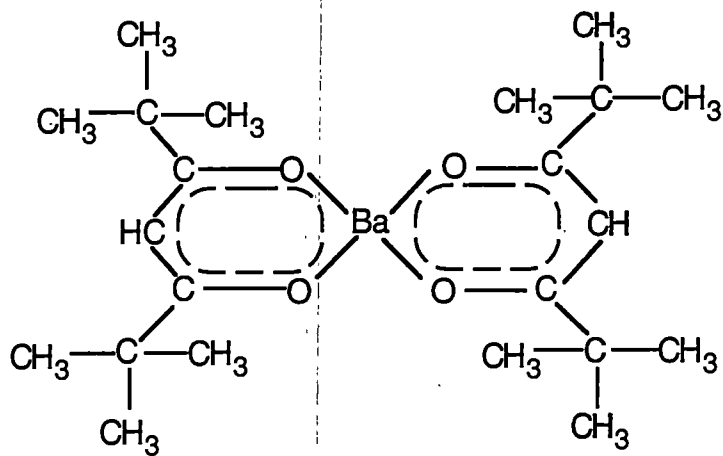
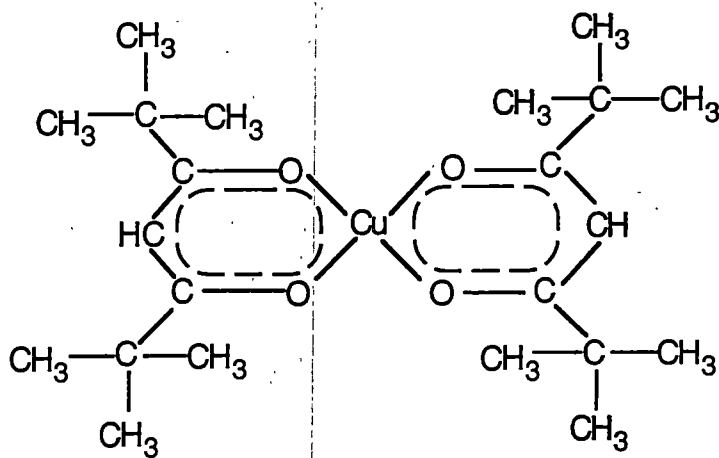


Figure 4. $\text{Cu}(\text{DPM})_2$ Reference Spectra [17].



(a) Structure of $\text{Ba}(\text{TMHD})_2$



(b) Structure of $\text{Cu}(\text{TMHD})_2$

Figure 5. Precursor Structure Diagrams [15].

CHAPTER III

EXPERIMENTAL ANALYSIS

Experimental Apparatus

The experimental setup utilized common absorption spectroscopy techniques to meet the experimental objectives. These objectives included defining detailed gas phase absorption spectra of each precursor at MOCVD vacuum conditions, selecting measurement wavelengths for each precursor and defining associated Beer's law constants, and examining vaporization characteristics to determine if temperature can be used to control conditions. Figure 6 provides an illustration of the experimental setup. The literature search indicated that strong spectral absorption for all of the TMHD precursors would be observable in the ultraviolet region, 200nm to 400nm. A deuterium lamp with its strong ultraviolet output was the light source. Collimating lenses and apertures served to collimate the ultraviolet light into a 0.5 inch diameter beam.

Precursor vaporization took place in a controlled temperature oven capable of temperatures up to approximately 300°C and maintaining a steady temperature to within $\pm 1^\circ\text{C}$. The oven temperature was monitored and controlled through the use of the oven temperature thermostats and a calibrated resistance thermometer. The resistance thermometer was placed in contact with the experimental vacuum (absorption) chamber. The temperature difference between the external temperature transducer and the oven thermostats was approximately (4-5)°C when heating and (1-2)°C when cooling. Constant oven temperatures at a particular thermostat setting were attainable after a (30-45)min warm-up time. The resistance thermometer readings provided the temperatures presented in the data of all absorption experiments.

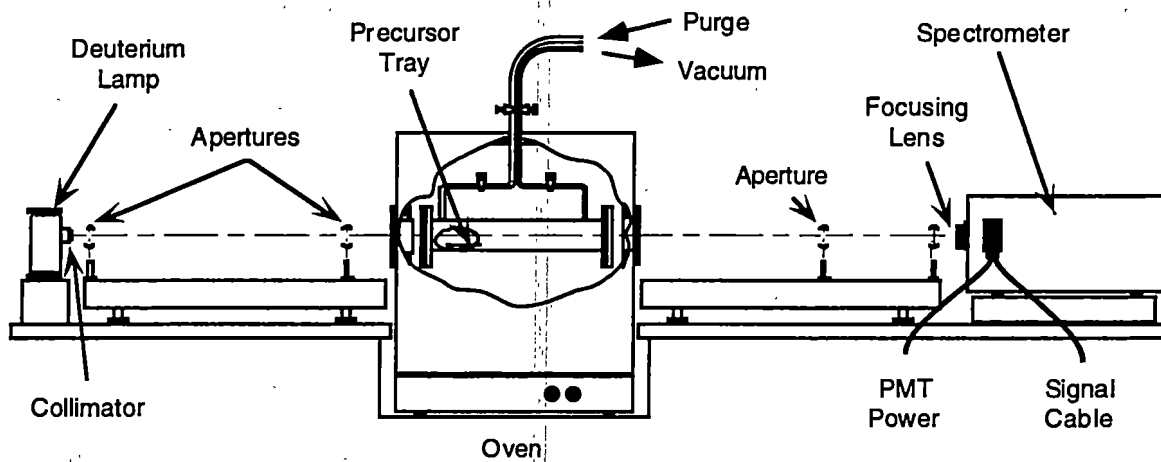


Figure 6. Experimental Setup.

The absorption or vacuum chamber in which the precursor samples were vaporized was housed in the interior of the oven. Figure 7 shows the dimensions of the absorption chamber. A precursor tray with a cylindrical base and an attachable top was the sample container. The length of the stainless steel vacuum chamber was approximately 20 inches (50.8cm). This length also served as the absorption pathlength b . The vacuum chamber was sealed through the use of windowed flanges whose inner diameters contained sapphire windows for transmitting the ultraviolet beam through the chamber during the vaporization studies. Sapphire windows were also mounted onto the sides of the oven such that the UV light could be transmitted through the oven and into the absorption chamber while maintaining a uniform oven temperature. Additionally, argon purge plumbing and vacuum valves were connected to the chamber such that initiating vacuum conditions or purging the chamber with argon were easily accomplished.

The vacuum chamber pressure was monitored by utilizing a capacitance manometer and a (0-150)Torr Bourdon gauge used to indicate the pressure range. The capacitance manometer measured pressures within 1×10^{-4} Torr and was calibrated against the Bourdon gauge calibration. The offset between the two pressure gauges was about 1.00Torr because the gauge indicator was adjusted when it was calibrated. Since MOCVD vaporization of barium, copper, and yttrium precursors are conducted at pressures of (0-10)Torr, a vacuum pump capable of attaining a pressure down to approximately 0.03Torr, was utilized in the experimentation to simulate MOCVD pressure conditions. Pressure readings from the capacitance manometer were recorded using a National Instruments AID board and a LabVIEW software program that provided the pressure data reported in the results.

The experimental setup can be described in the following succinct manner. The deuterium source produces broad band UV light, which is collimated to a 0.5 inch (1.27cm) beam diameter. The collimated UV beam is transmitted through the oven and

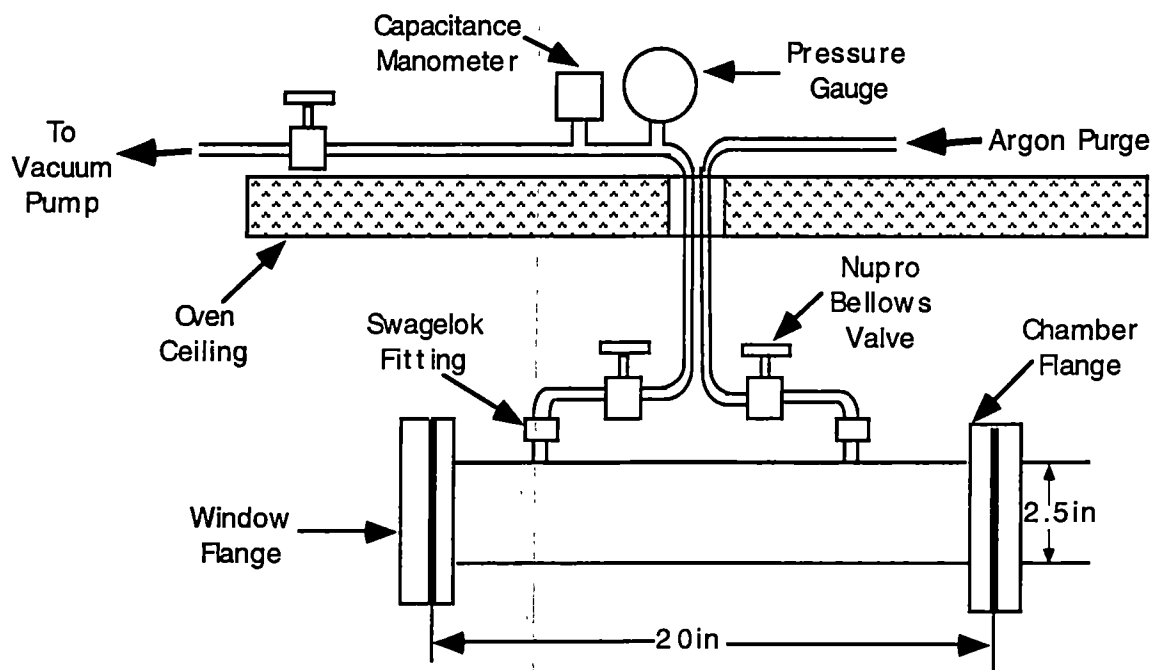


Figure 7. Absorption Chamber Dimensions.

absorption chamber windows. The UV beam that passes through the empty chamber at baseline conditions represents the I_0 , or baseline intensity measurement. The I , or transmission intensity measurement results from photons in the incident beam being absorbed by atoms of vapor in the chamber when the TMHD precursors are vaporized. The absorption is the difference between the two measurements, and varies with wavelength as a function of the characteristic absorption bands of the TMHD precursors. Collimation optics focus the broad band beam on the entrance slit of the spectrometer so that light intensity can be measured as a function of wavelength.

An Acton Research Corporation SpectraPro-500 0.5 meter triple grating spectrometer/monochromator was used to acquire the transmission data. The stepper motor-driven spectrometer has multiple gratings allowing use in the UV, visible, and infrared wavelength regions. The 2400g/mm UV grating, with a minimum resolution of 0.025nm for a 10 μ m slit, was the grating used in the experimentation. Other features of the spectrometer include a Czerny-Turner type optical system, f/6.9 aperture ratio, ± 0.1 nm wavelength accuracy, and ± 0.025 nm wavelength reproducibility. The spectrometer's detector was a photomultiplier tube featuring a thermoelectric cooler. The monochromator was controlled through the LabVIEW software program with an IEEE-488 interface to the Actor stepper motor controller. The National Instruments board was used to digitize the spectrometer photomultiplier signal, converted from a current to a voltage signal with a low input impedance amplifier/noise filter. Delays inherent in the Actor stepper motor controller/feedback module could be accommodated in the LabVIEW software by stopping the spectrometer at each desired measurement wavelength, or in data analysis by aligning known source lines with output wavelengths.

Experimental Calibration

Several system calibrations were conducted prior to initiating the YBCO precursor vaporization experiments. Both spectrometric and pressure instrumentation were calibrated and a calibrated resistance thermometer was the primary temperature sensor.

The spectrometer calibration consisted of identifying known mercury lines using a mercury pin lamp. Sixteen mercury lines between 237nm and 546nm were used. Additionally, three of these mercury lines greater than 400nm were measured using the room lights as the mercury light source. Typical mercury lines at 253.652nm, 404.656nm, and 435.833nm are shown in Figures 8, 9, and 10, respectively. Figure 11 shows the results of the spectrometer calibration. The entrance and exit slit settings on the spectrometer were set at 20 μ m, half of what was used for the MOCVD precursors, for these measurements of the mercury lines.

Figures 8, 9, and 10 show the measurement of the 253.652nm, 404.656nm, and 435.833nm mercury spectral lines, respectively. The wavelength shift between the actual 253.652nm mercury line and the measured result was 0.022nm. The wavelength shift between the actual 404.656nm mercury line and the measured result was 0.036nm. The wavelength shift between the actual 435.833nm mercury line and the measured result was 0.043nm. The wavelength shifts were due to mechanical and optical tolerance effects. Lastly, graphical analysis of Figures 8, 9, and 10 indicate a 0.035nm spectrometer resolution using 20 μ m slit widths, which is slightly better than the minimum specified spectrometer resolution. Figure 11 shows the results of the spectrometer calibration using all measured mercury spectral lines. Figure 11a shows there is no regular shift in the spectrometer wavelength measurements. The variance data in Figure 11b show that the spectrometer measurements of mercury lines in the 200nm to 400nm region, the wavelength interval in which the precursor absorption data were taken, randomly vary by ± 0.02 nm, within the stated accuracy of the spectrometer. The spectrometer data collection

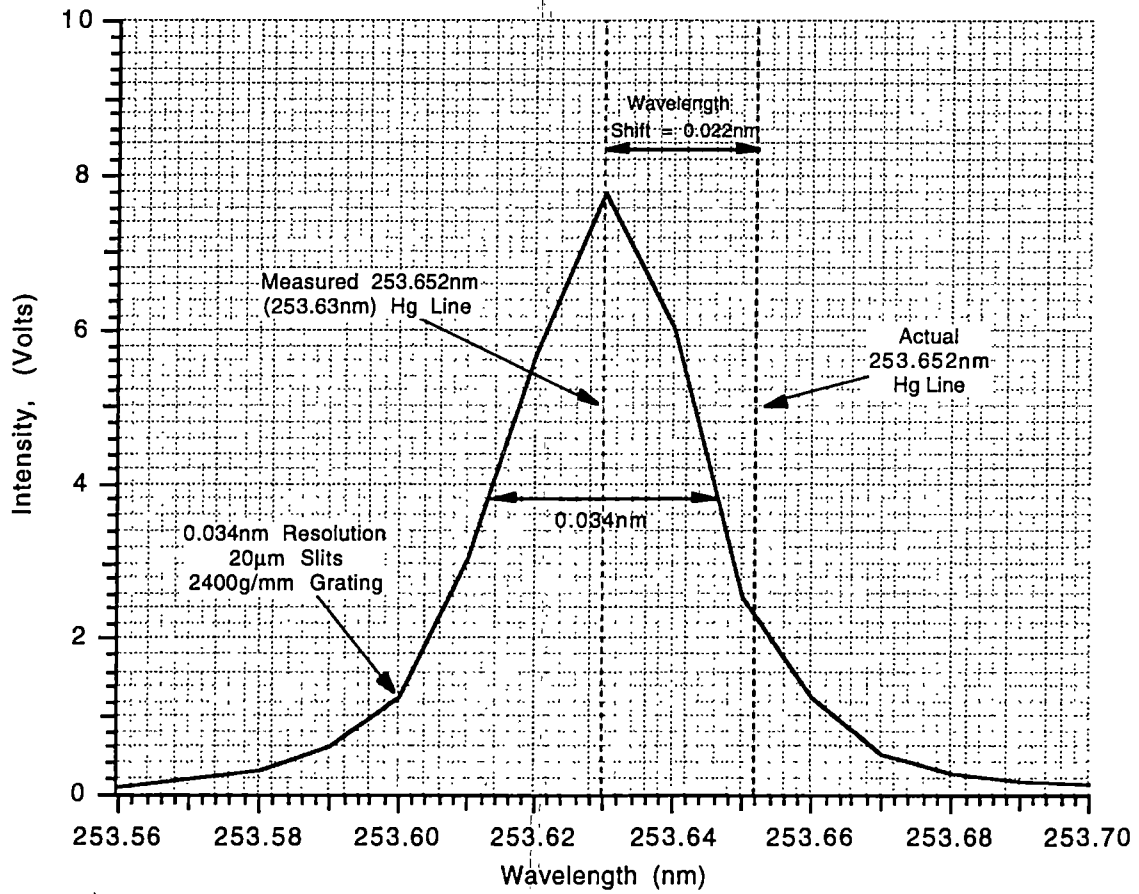


Figure 8. Spectrometer Calibration of 253.652nm Mercury (Hg) Spectral Line.

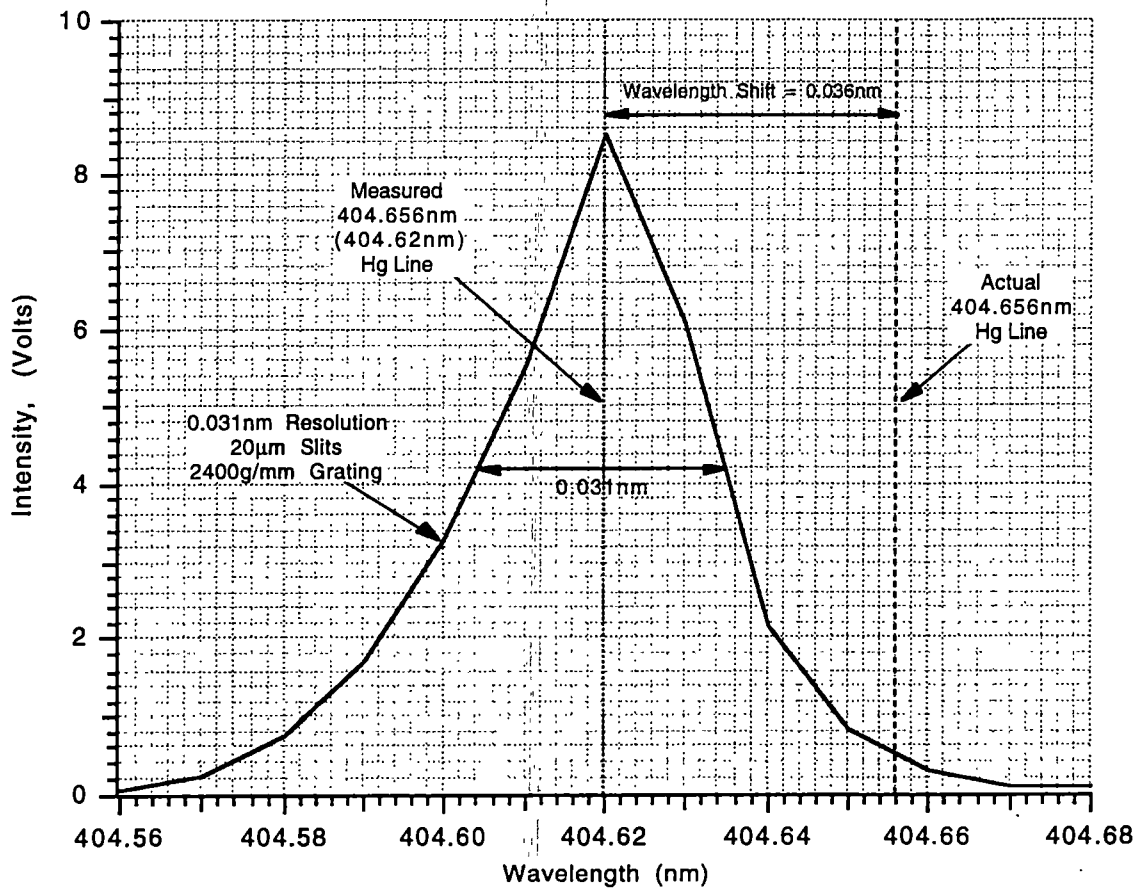


Figure 9. Spectrometer Calibration of 404.656nm Mercury (Hg) Spectral Line.

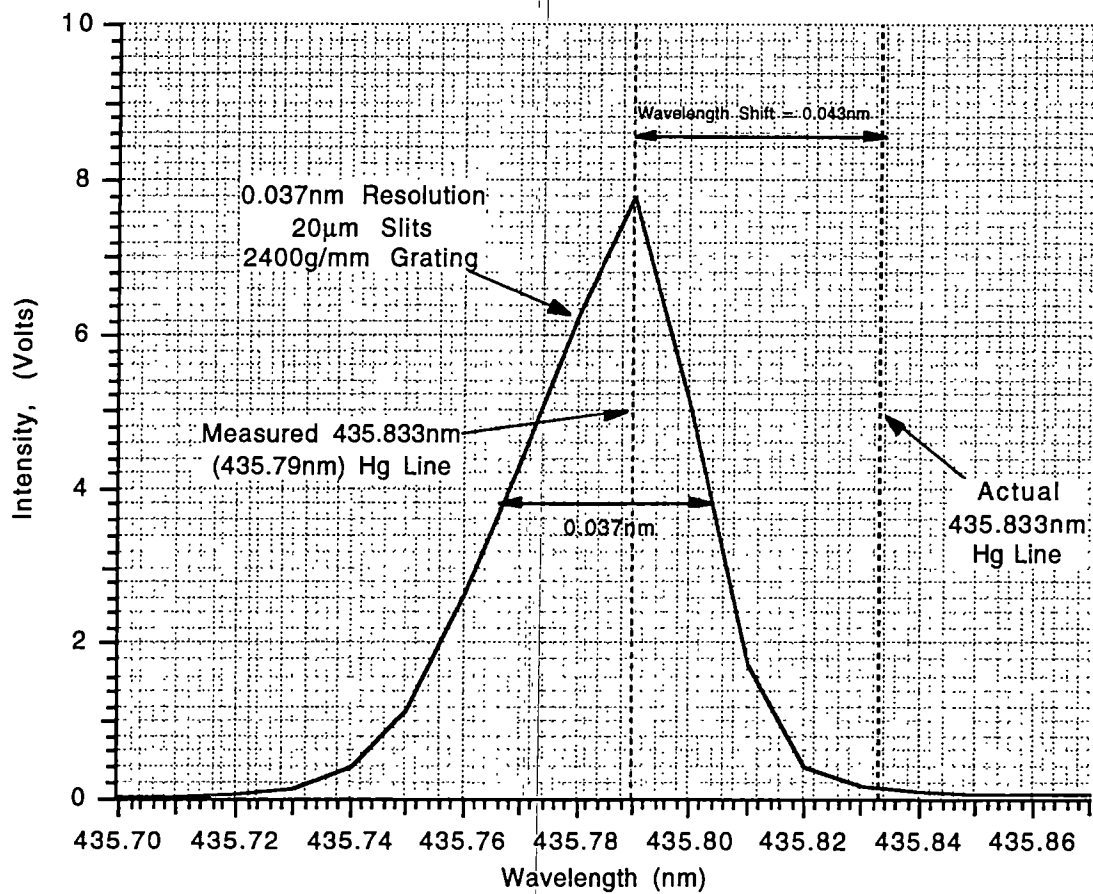
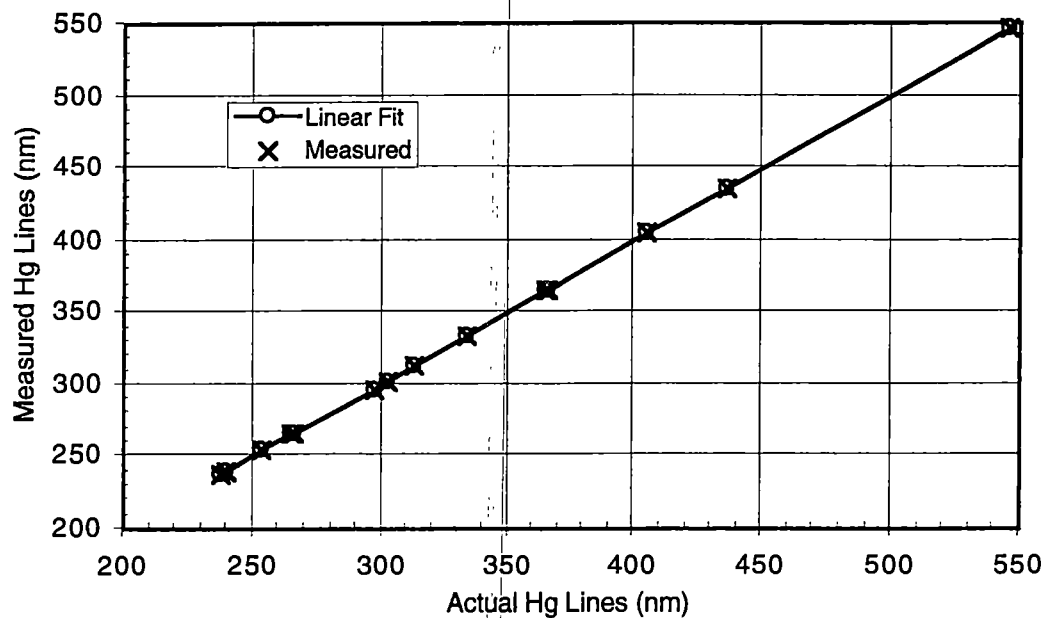
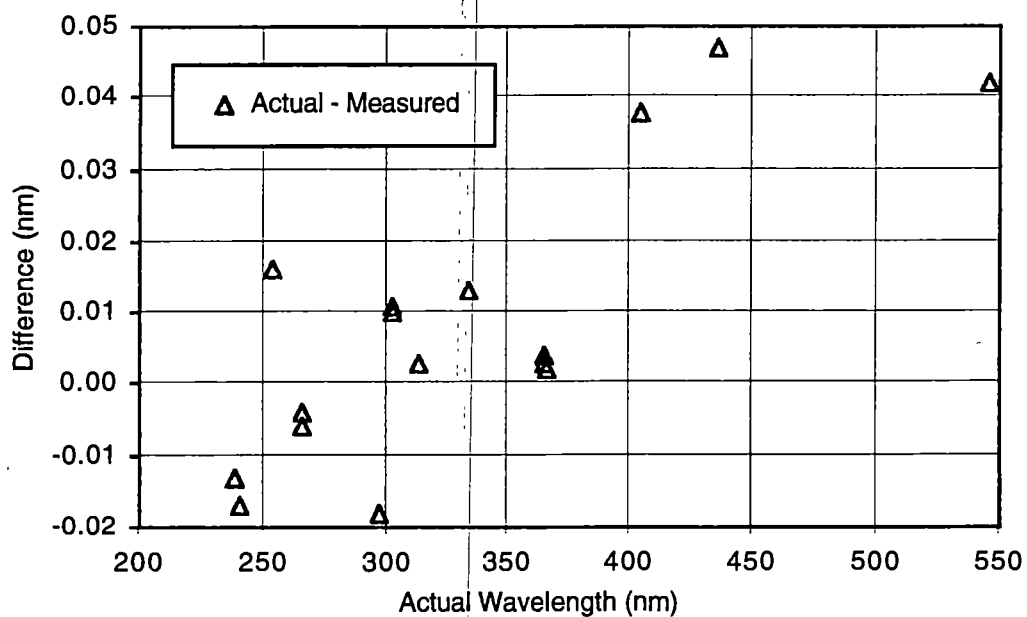


Figure 10. Spectrometer Calibration of 435.833nm Mercury (Hg) Spectral Line.



(a) Acton Spectrometer Calibration



(b) Acton Spectrometer Wavelength Variance

Figure 11. Spectrometer Calibration Data.

program has two scanning data collection capabilities. One is point-by-point or stop and go data collection. Using the point-by-point data collection, the spectrometer is set to the desired wavelength and then data is collected. This procedure is then repeated to cover the wavelength interval in question. The other data collection method used by the program involves scanning a wavelength interval at a specified scanning speed, while continuously acquiring data. The stop and go scanning option produces the more dependable wavelength determination. However, a lengthy scanning time is required with this method because of the slow feedback from the spectrometer controller. This results in over 5.5h scan time for one stop and go detailed precursor absorption scan from 200nm to 400nm. Therefore, the continuous scanning option was utilized in all absorption scans. Known deuterium lines which are in the scans were used to accurately determine the absolute wavelengths in the continuous scans.

Finally, measurement of the well-known UV absorption spectrum of NO was used to evaluate the absorption measurement procedures before conducting the precursor absorption experiments. The NO absorption spectra were taken at various pressures in the absorption chamber. This resulted in the measurement of NO absorption spectra at partial pressures of 0.05, 0.10, and 0.15Torr, which showed the expected near linear absorption versus concentration relationship. These results are presented in Figures 12 and 13. Figure 12 indicates that absorbance increases with an increase in NO pressure. This is expected since an increase in NO pressure implies an increase in the NO concentration in the absorption chamber. Figure 13 further illustrates this point using the ratio of NO absorbance as a function of wavelength. Figure 13 illustrates the expected result of the ratio of NO absorbance increasing with an increase in the NO partial pressure ratio.

The capacitance manometer and pressure gauge were also calibrated. A linear fit of the pressure gauge readings to the "actual" NIST traceable calibration pressures is presented in Figure 14 and the calibration of the capacitance manometer, using the pressure

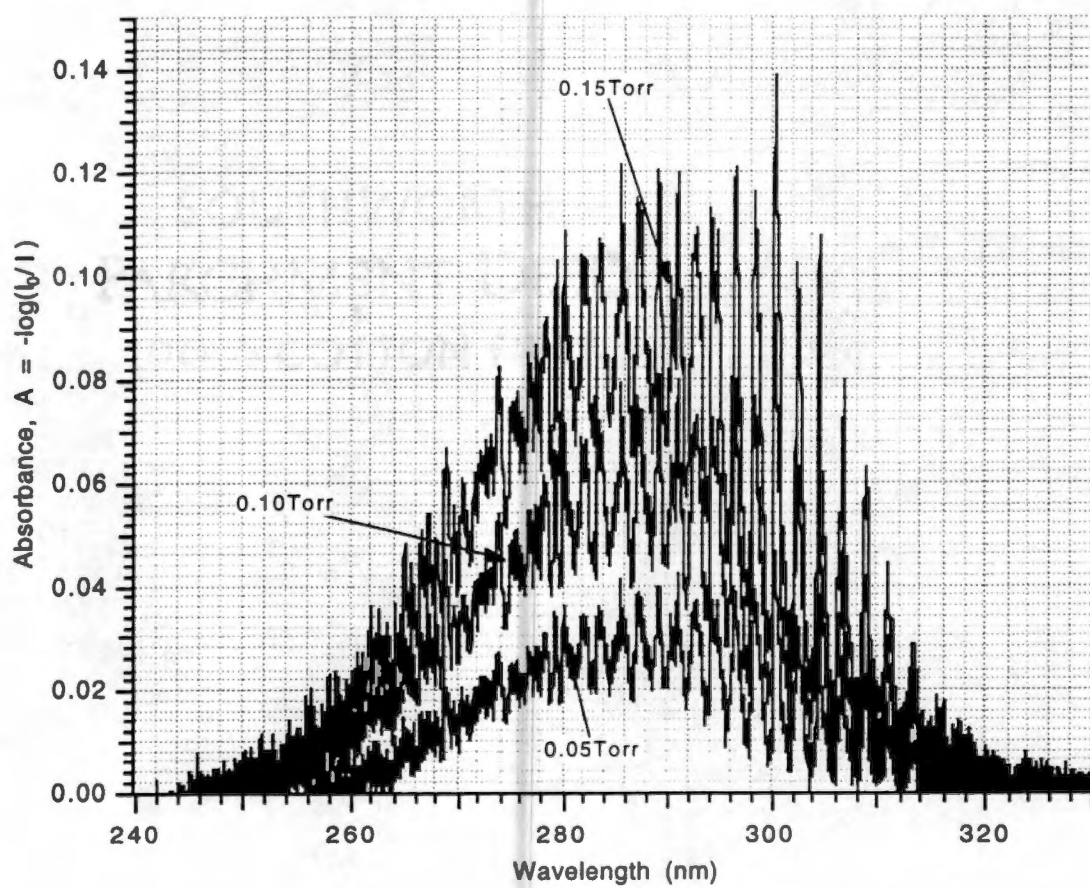


Figure 12. Absorption of NO Gas at 0.05Torr, 0.10Torr, and 0.15Torr.

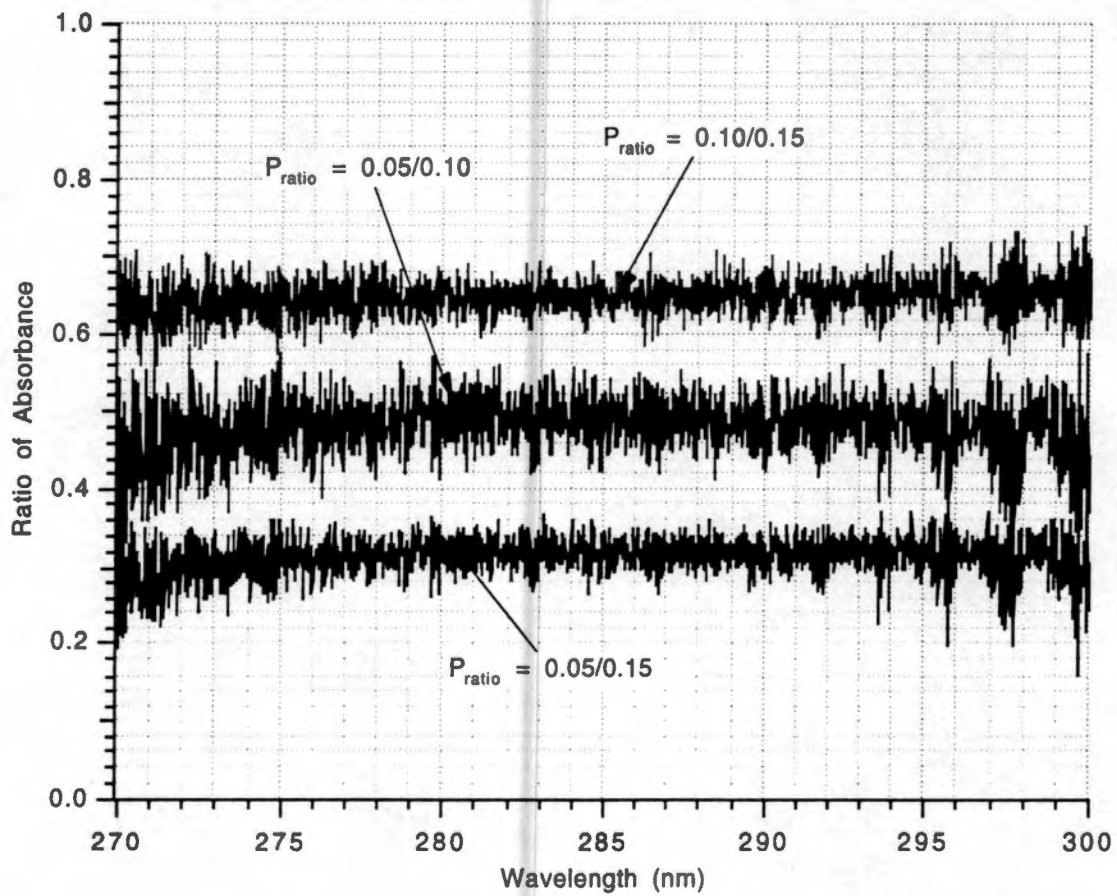
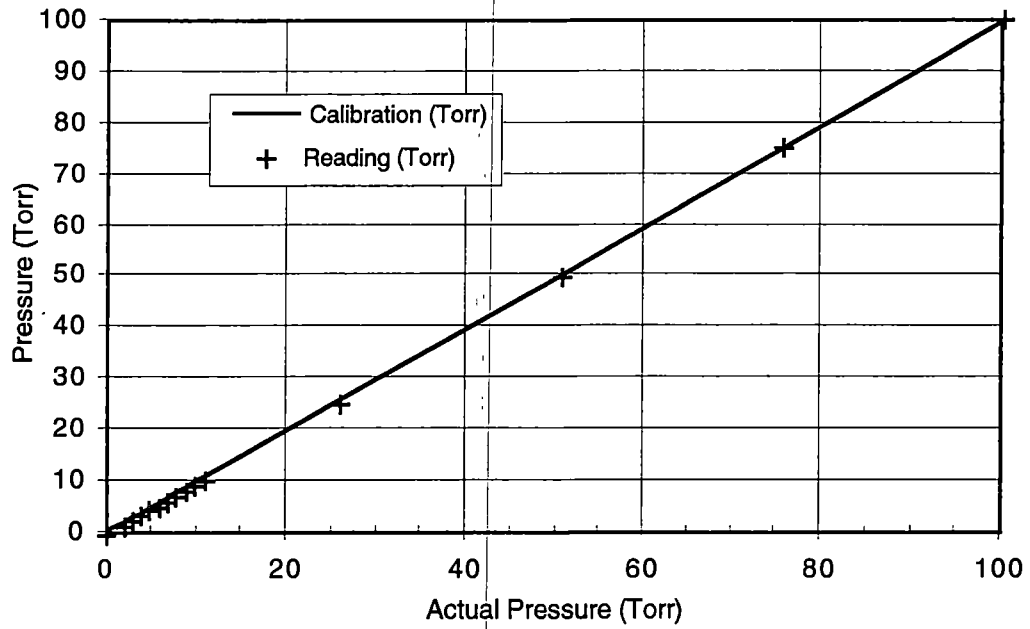
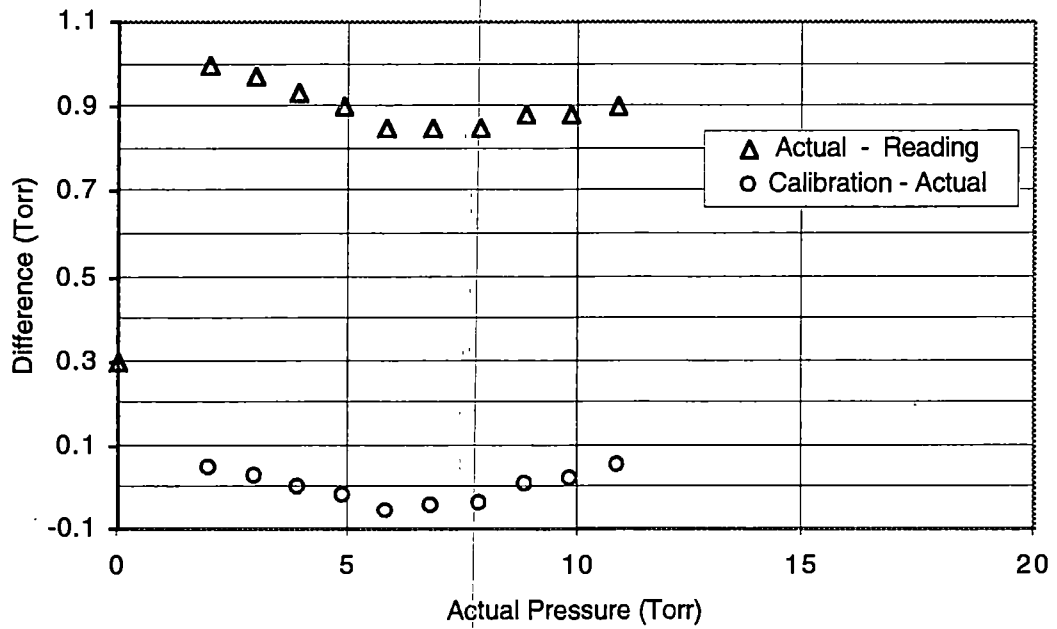


Figure 13. Absorbance Ratios of NO Gas.



(a) Pressure Gauge Calibration



(b) Pressure Gauge Calibration Variance

Figure 14. Pressure Gauge Calibration Data.

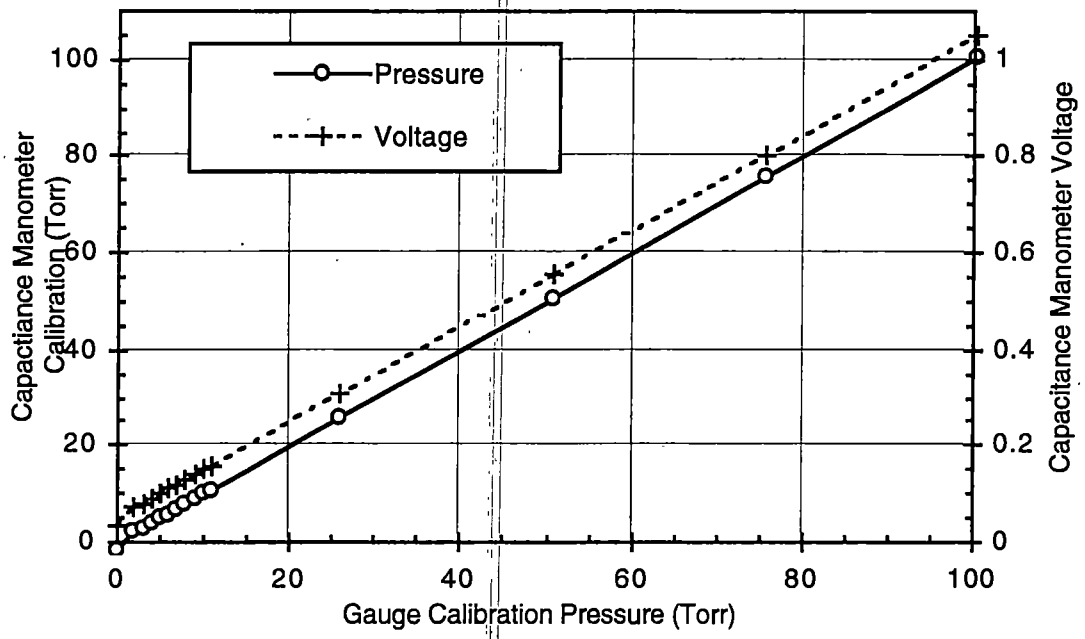
gauge as a transfer standard, is presented in Figure 15. The offset between the pressure gauge readings and capacitance manometer is approximately 1Torr, in the 0.1Torr to 10Torr regime of interest, and the pressure readings from the capacitance manometer were the pressure data presented in the results.

Experimental Precursor Absorption Procedures

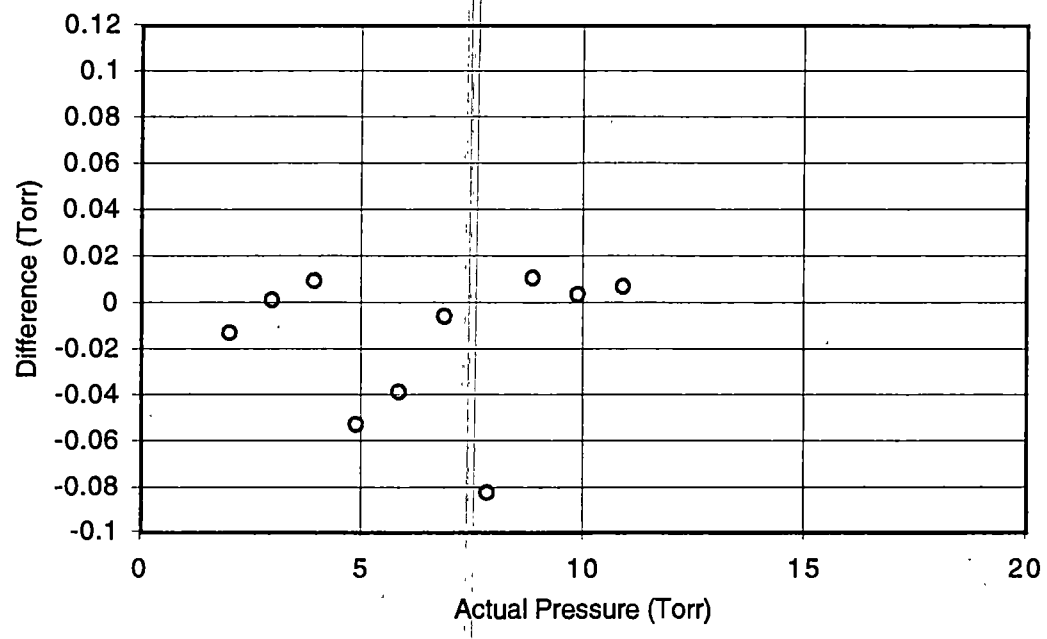
This section describes the steps utilized in measuring and analyzing the absorption spectra of the vaporized TMHD complexes of copper, yttrium, and barium.

Pre-test system preparation was a crucial element of the absorption analyses. The deuterium source was scanned prior to each test to ensure that optical alignment was maintained, as indicated by no decrease in empty cell light transmission of the collimated ultraviolet beam. A warm-up period of about one hour was employed to allow the deuterium source to reach equilibrium conditions and produce stable measurements. Likewise, the photomultiplier tube cooler was kept at a constant 0°C for at least 24 hours before each test. To avoid contamination of the sapphire windows, spectroscopic grade acetone and methanol were used to clean the windows before and after each absorption scan.

Standard spectrometer parameters for all of the precursor absorption experiments were utilized. The entrance and exit slits of the spectrometer were set at 40 μ m to attain maximum UV light throughput, while maintaining good instrument resolution. As mentioned previously, the spectrometer resolution using 20 μ m slit settings was approximately 0.035nm (see Figures 6, 7, and 8). Therefore, the spectrometer resolution using 40 μ m slit settings was approximately 0.070nm. The voltage to the photomultiplier tube power supply was adjusted to yield a peak voltage for baseline transmission at just under 10V. Standard continuous mode scanning parameters were utilized in all of the



(a) Capacitance Manometer Calibration



(b) Capacitance Manometer Variance

Figure 15. Capacitance Manometer Calibration Data.

absorption I and baseline I_0 scans presented in the results. These standard scanning parameters were the following:

- scan speed = 3nm/min
- samples averaged = 1,000
- sample frequency = 10,000Hz
- scanning interval = (200-400)nm

These scanning parameters yielded an intensity signal averaged over every 0.005nm, thus providing 14 points per each 0.07nm resolvable line. The scanning time involved was approximately 70min per scan. The low resolution (fast) scans included all of the above parameters with the exception of using a scan speed of 300nm/min.

According to the literature, the TMHD complexes of barium, copper, and yttrium are easily contaminated outside of an inert, low moisture environment. Therefore, procedures for transporting the powders from an argon purged glove box to the argon purged absorption chamber were established. A sample container featuring a cylinder type base and removable, sealable top was utilized in transporting the samples. Additionally, plastic glove bags were set up next to the absorption system such that vacuum and argon environments could be created while loading the sample container into the chamber. The following steps were taken in transporting the precursor samples from the argon glove box to the absorption chamber and preparing for absorption experimentation:

1. Clean the vacuum chamber and sapphire windows.
2. Purge the empty chamber with alternating vacuum and argon flushing, finishing with an atmospheric pressure of argon and closed chamber valves.
3. Purge the plastic glove bag by subjecting it to alternating vacuum and argon flushing, before filling the plastic glove bag with argon.
4. In the glove box, weigh the empty sample container. Then, measure a quantity of a precursor sample in the sample container. Seal the sample container and remove sample container from the glove box.
5. Remove vacuum chamber from oven.

6. Place vacuum chamber and sample container in plastic glove bag, seal bag, and purge with vacuum and argon flushing.
7. Open vacuum chamber in glove bag. Remove top of sample container and install it in vacuum chamber. Seal vacuum chamber.
8. Remove vacuum chamber from plastic glove bag. Attach vacuum chamber to vacuum and argon connections in oven. Subject chamber to vacuum conditions, (0-5)Torr and close valves at vacuum chamber inlet.
9. Perform absorption experiments.

The procedure used in scanning the absorption spectra of the precursors involved heating the sample gradually. Several fast (300nm/min) scans were conducted while the oven temperature increased. Temperature, pressure, and absorption data were recorded during the heating process and during all absorption experiments. This technique permitted a determination of the temperature and pressure ranges at which the precursors began to vaporize; once they began to vaporize the temperature was held constant. When the absorption of the precursor sample under study became stable at the set temperature, then a 3nm/min transmission scan was recorded. Stable absorption conditions were usually achieved in approximately one hour after the oven was set to a constant temperature. After the detailed absorption scan was completed, the temperature was increased to observe if further absorption would occur. Additional fast scans were conducted during this heating period and temperature, pressure, and absorption data were recorded. This technique produced a good approximation of temperature ranges at which the samples became fully vaporized. Figure 16 shows the $Y(TMHD)_3$ transmitted intensity as a function of temperature data used in determining the $Y(TMHD)_3$ initial and complete vaporization temperature estimates. Also, Figure 17 shows the $Y(TMHD)_3$ transmitted intensity as a function of time data collected to observe stable vaporization prior to conducting the detailed transmission scan at a constant temperature of (123-124) $^{\circ}C$. For the $Cu(TMHD)_2$ and $Y(TMHD)_3$ no increases in absorption were observed during this heating period, so it was deduced that the $Cu(TMHD)_2$ and $Y(TMHD)_3$ had fully vaporized prior to recording

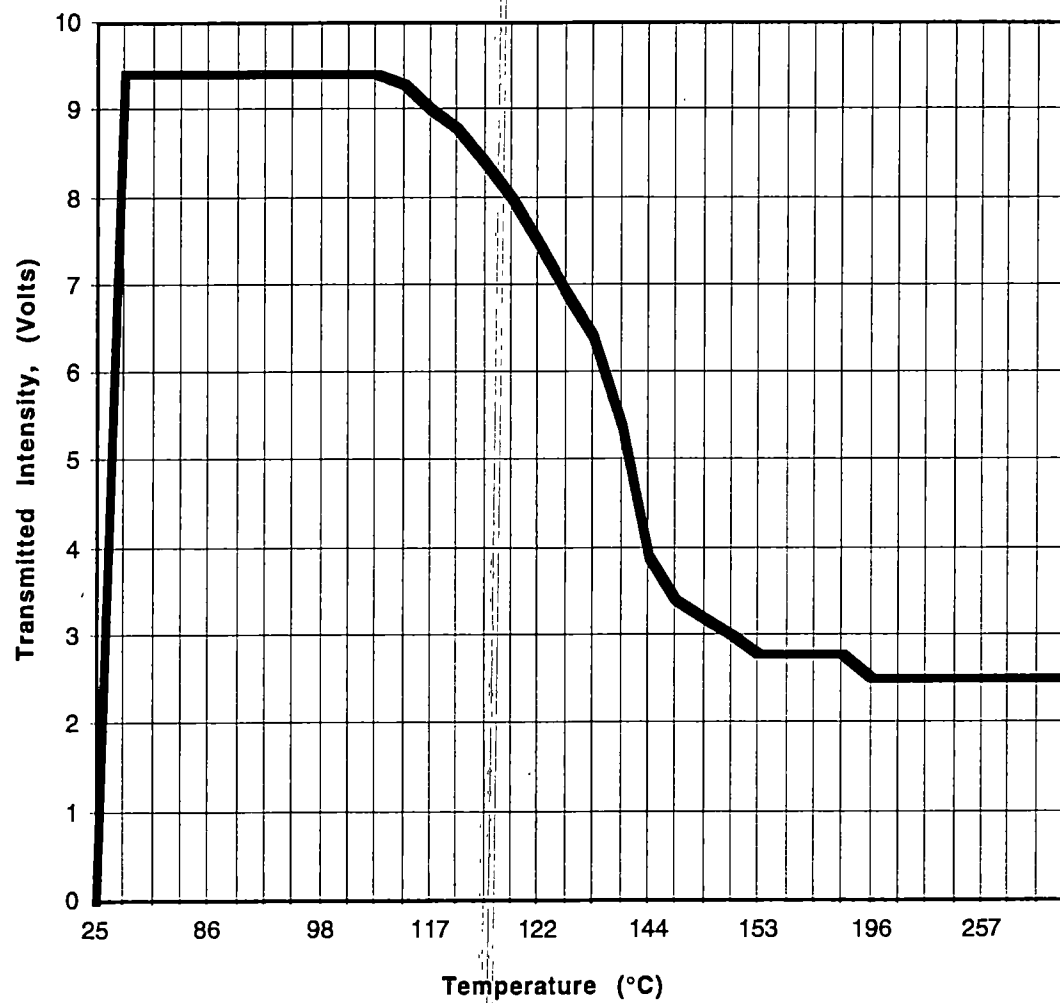


Figure 16. $Y(TMHD)_3$ Transmitted Intensity as a Function of Temperature.

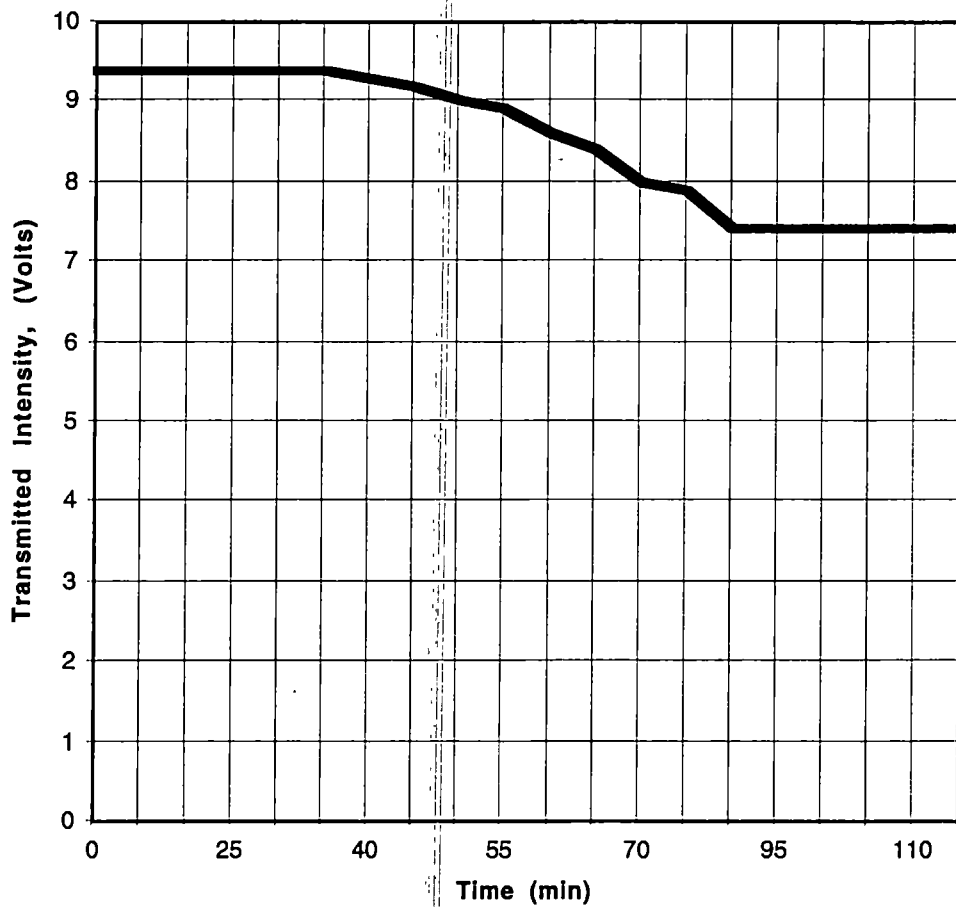


Figure 17. $Y(TMHD)_3$ Transmitted Intensity as a Function of Time.

the transmission scans. The Ba(TMHD)_2 showed an increase in absorption with further heating, and unlike the Cu(TMHD)_2 and Y(TMHD)_3 , some Ba(TMHD)_2 remained in the sample container after the chamber was cooled. Therefore, the Ba(TMHD)_2 scan was repeated, and the chamber was sealed and cooled immediately after completion of the transmission scan, so that the remaining sample could be weighed to determine the mass of vaporized Ba(TMHD)_2 . (The Cu(TMHD)_2 and Y(TMHD)_3 sample containers were also weighed right after cooling, and showed no measurable compound remained.) Post-vaporization measurements were also conducted. After the vaporization experiments were conducted, the absorption chamber was purged with argon and any remaining vapor remaining in the chamber was vacuumed from the chamber. After removing the sample tray from the chamber, a standard high resolution baseline I_0 scan was taken of the UV light at the temperature at which the detailed absorption scan had been taken. This was needed to get an accurate reference light signal level since the sapphire windows have a slight transmission decrease with temperature for wavelengths below 230nm. Extensive scanning of the UV I_0 light transmission at atmospheric pressure, vacuum pressure, and high temperatures, clearly indicated that only temperature caused changes in the output of the baseline I_0 curve. Consequently, an accurate Beer's law calculation could be made for the extinction coefficient a using I_0 = detailed temperature baseline scan, I = detailed absorption scan, C = concentration of material vaporized, and b = absorption pathlength (50.8cm). All scans were run in a darkened room, but to eliminate any background light effects a background I_b scan was also run for each precursor scan with the deuterium lamp off, but with the photomultiplier at 0°C and at the appropriate voltage.

The absorbance as a function of wavelength was graphically represented by utilizing the relationship between transmission and absorbance.

$$\text{Absorbance} = -\log_{10}(I/I_0) \quad (14)$$

where

$$I = \text{Transmission Chamber Scan} - \text{Background Scan} \quad (15)$$

was used for both baseline I_0 and precursor I transmission.

Sources of Error

Possible sources of experimental error will be discussed in this section. Most of the potential error arose either from the transport of the precursor samples from the argon glove box environment and the absorption chamber or from other experimental difficulties. Measurement uncertainties due to limitations in measurement precision and bias will also be discussed.

Contamination of the precursor samples while transporting them from the argon glove box to the absorption chamber is one source of error. The exposure of the sample to ambient conditions during the transporting process must be minimized to reduce any potential sample contamination, especially from water vapor. This issue was experimentally rectified through the use of the precursor sample tray and transporting the sample into the absorption chamber in an argon-filled glove bag. However, the samples tested have been used for other experiments, subjecting them to possible unknown contamination.

A gradual vacuum leak through the window flanges was observed at times during operation at vacuum. Several attempts were made to solve this problem. Employing an aggressive torqueing pattern on the flange bolts and utilizing soft copper seals on the window flanges did not completely eliminate the vacuum leak. Therefore, at stable absorption conditions, a pressure rise of (1-2)Torr during the one to two hour scanning needs to be noted.

The optical alignment of the UV beam experienced changes due to an inability to securely fix positions of all optical elements with available equipment. This was primarily a result of the lack of availability to an optical table on which the optical devices could be

securely anchored. Optical alignment checks of the UV beam prior to and following conducting each absorption experiment was used to assure that no alignment shifts occurred during the experiments.

The baseline I_0 curves and the transmission I curves were recorded as photomultiplier tube volts as a function of wavelength. The voltage measurements were made with a resolution of 4.88mV. The upper bound of the voltage scale on the data collection program was 10.0V. Therefore, the goal of the I_0 scans was to have the output of the peak of the baseline curve as close to 10.0V as possible. This was accomplished after optical alignment of the UV beam prior to each set of precursor absorption experiments by adjusting the voltage setting of the photomultiplier tube power supply to yield a nearly 10V detector output at the maximum I_0 light intensity wavelengths for an unheated chamber. The I_0 scans were taken at the temperature setting at which the detailed precursor absorption I scans were taken.

Initial precursor absorption experiments indicated that the absorption pathlength b of 50.8cm was too long. This conclusion was based on the results of excessive absorption of precursor samples greater than 0.01g and the fact that the absorbance A is directly proportional to the absorption pathlength b . Therefore, the precursor sample mass had to be reduced to (0.0005-0.0050)g and gradual heating of the samples was initiated, with the intent of stopping vaporization by holding the temperature constant at a fixed level of absorption. However, as mentioned previously, the samples continued to vaporize, even though the temperature was not increased. Detailed scans were only recorded once the transmitted signal level quit changing. This required holding the sample chamber at constant temperature for almost an hour, but in that time all the Cu(TMHD)_2 and Y(TMHD)_3 samples vaporized and a significant portion of the Ba(TMHD)_2 sample also vaporized. The only means to limit absorbance to measurable levels was to limit the

precursor sample masses, and the precision of the scale available to measure the masses was 0.00005g.

The species molecular weight M was known to ± 0.001 g/mol and the chamber volume V was known to 0.005L. This resulted in a ΔC precision uncertainty in the measured concentration of each precursor using

$$C = \frac{m}{MV} \quad (16)$$

$$\Delta C_p \equiv \left| \frac{\partial C}{\partial m} \right| \Delta m + \left| \frac{\partial C}{\partial M} \right| \Delta M + \left| \frac{\partial C}{\partial V} \right| \Delta V \quad (17)$$

$$\Delta C_p = \frac{1}{MV}_{species} (0.00005) + \frac{m}{M^2V} (0.001) + \frac{m}{MV^2} (0.005) \quad (18)$$

Table 2 lists the resulting precision uncertainties for each precursor, with the chamber volume measured as 1.47L.

Biases can be estimated similarly assuming the scale can be biased by as much as 0.0001g, and the volume measurement can be biased by 0.005L. Bias estimates are given in Table 2 as ΔC_b . Concentration uncertainties ΔC are given with 95% confidence as

$$\Delta C = 2 * \Delta C_p + \Delta C_b \quad (19)$$

Of course, if the precursor vapor pressures were greater than anticipated and significant mass of precursor vaporized when the chamber was evacuated, significantly greater errors would occur in the concentration measurements. All concentration uncertainties propagate to extinction coefficient a uncertainties. The significant percent concentration uncertainties, therefore, need to be reduced before accurate precursor extinction coefficients can be determined, and more accurate measurements of vaporized precursor mass is recommended for future work.

Table 2. Precursor Precision Uncertainties.

Precursor Sample	Vapor Mass, m (g)	Molecular Weight, M (g/mol)	Concentration, C ($\mu\text{mol dm}^{-3}$)	Concentration Precision Uncertainty, ΔC_p ($\mu\text{mol dm}^{-3}$)	Concentration Bias Uncertainty, ΔC_b ($\mu\text{mol dm}^{-3}$)	Concentration Uncertainty, ΔC ($\mu\text{mol dm}^{-3}$)
Cu(TMHD) ₂	0.0008	430.09	1.27	± 0.08	± 0.16	0.32
Y(TMHD) ₃	0.0012	638.73	1.28	± 0.06	± 0.12	0.24
Ba(TMHD) ₂	0.0022	503.89	2.97	± 0.08	± 0.16	0.32

Lastly, a noise anomaly appeared in the spectrometer scans. Extensive investigations resulted in concluding that the electrical components of the spectrometer scanning motor were the cause of the noise anomaly. This problem was rectified by significant averaging of the acquired scan points, as well as substantial noise filtering of the photomultiplier tube signal. An alternate software noise pulse filtering routine was also written, but it was found to be unneeded with the averaging and noise filtering.

CHAPTER IV

EXPERIMENTAL RESULTS

Cu(TMHD)₂ Absorption Experimental Results

Because of its lower vaporization temperature as determined in prior thermal gravimetric analysis, the Cu(TMHD)₂ precursor sample was the first sample analyzed using the absorption system. Thermogravimetric analysis curves for the three precursor samples used in this study are presented in Figures 18, 19, and 20. Initial vaporization tests of Cu(TMHD)₂ involved a 0.01g sample of the Cu(TMHD)₂ precursor, but this sample mass proved to be too absorptive to analyze in the 50.8cm long sample chamber. At the oven set temperature of 225°C, a value selected for significant vaporization from the thermogravimetric curve for Cu(TMHD)₂ [18], this sample quantity absorbed all the incident light in the Cu(TMHD)₂ absorption bands and detailed absorbance versus concentration measurements were not possible.

The next Cu(TMHD)₂ absorption experiment used a 0.0015g precursor sample. The results of these scans showed that vaporization of the sample began to occur in the (90-95)°C temperature range, considerably below onset of vaporization in the thermogravimetric analysis [14, 18]. Gradually increasing the temperature showed that maximum vaporization occurred between (145-155)°C as indicated by a lack of further changes in the absorption. This indicates that the sample is completely vaporized by 155°C utilizing constantly increasing temperatures in a less than 5Torr vacuum. This was further verified by the lack of remnants of the Cu(TMHD)₂ precursor following completion of the absorption analysis. Our thermogravimetric analysis and thermogravimetric data in the literature supported the complete vaporization of the copper precursor [14, 18]. However, all the thermal analysis data indicated complete vaporization of the copper precursor to

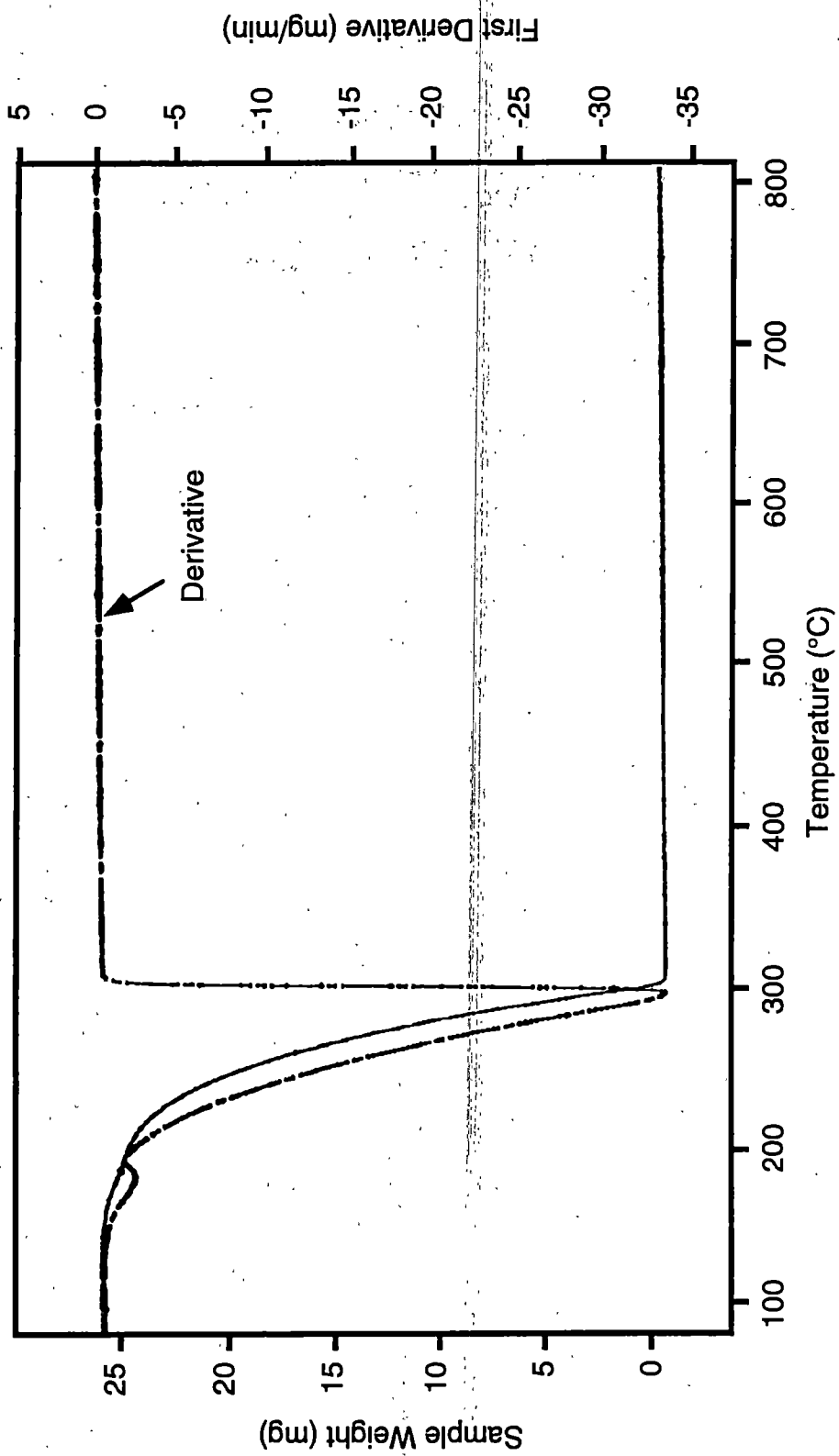


Figure 18. Cu(TMHD)_2 Thermogravimetric Analysis [18].

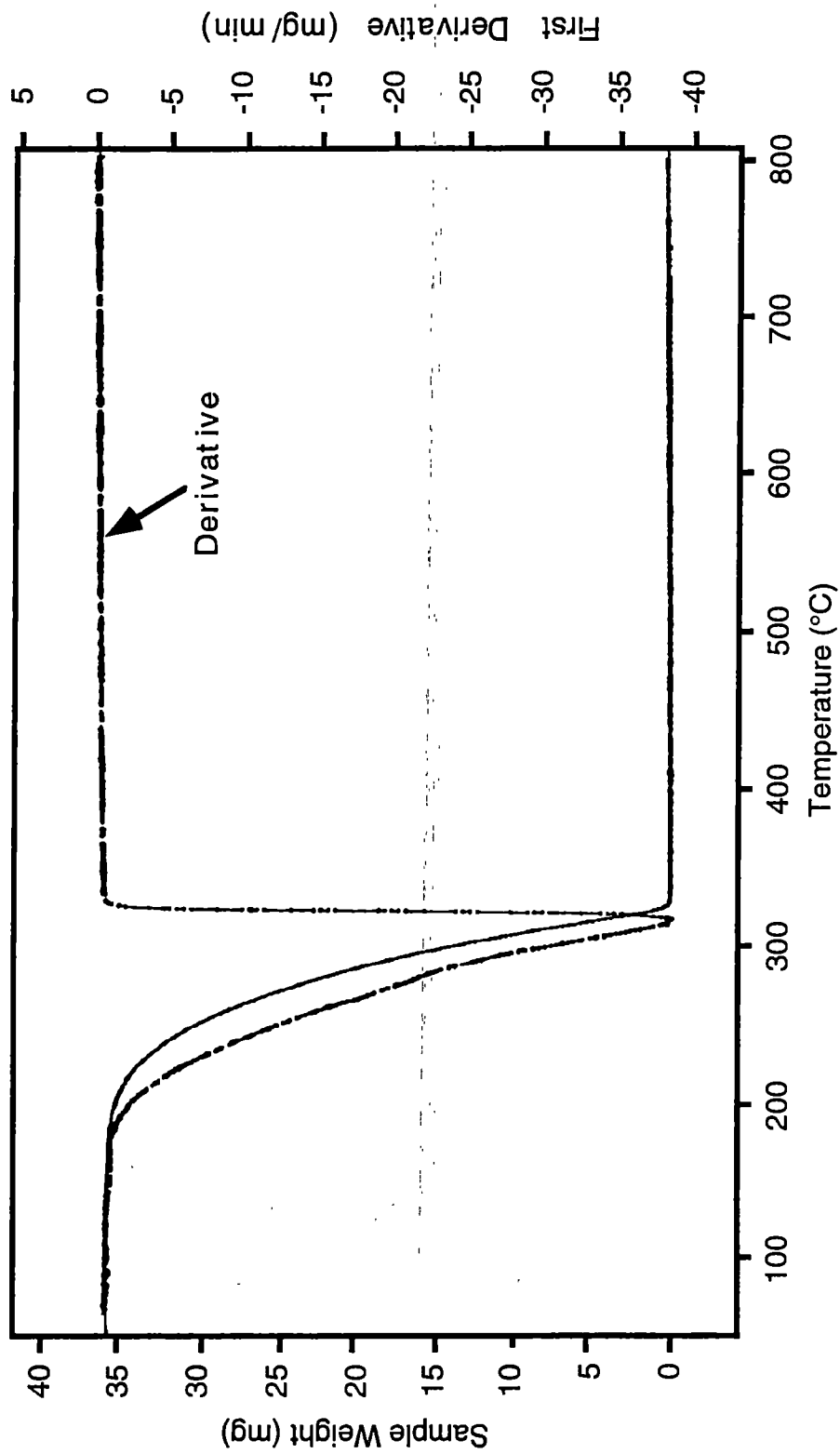


Figure 19. $Y(TMHD)_3$ Thermogravimetric Analysis [18].

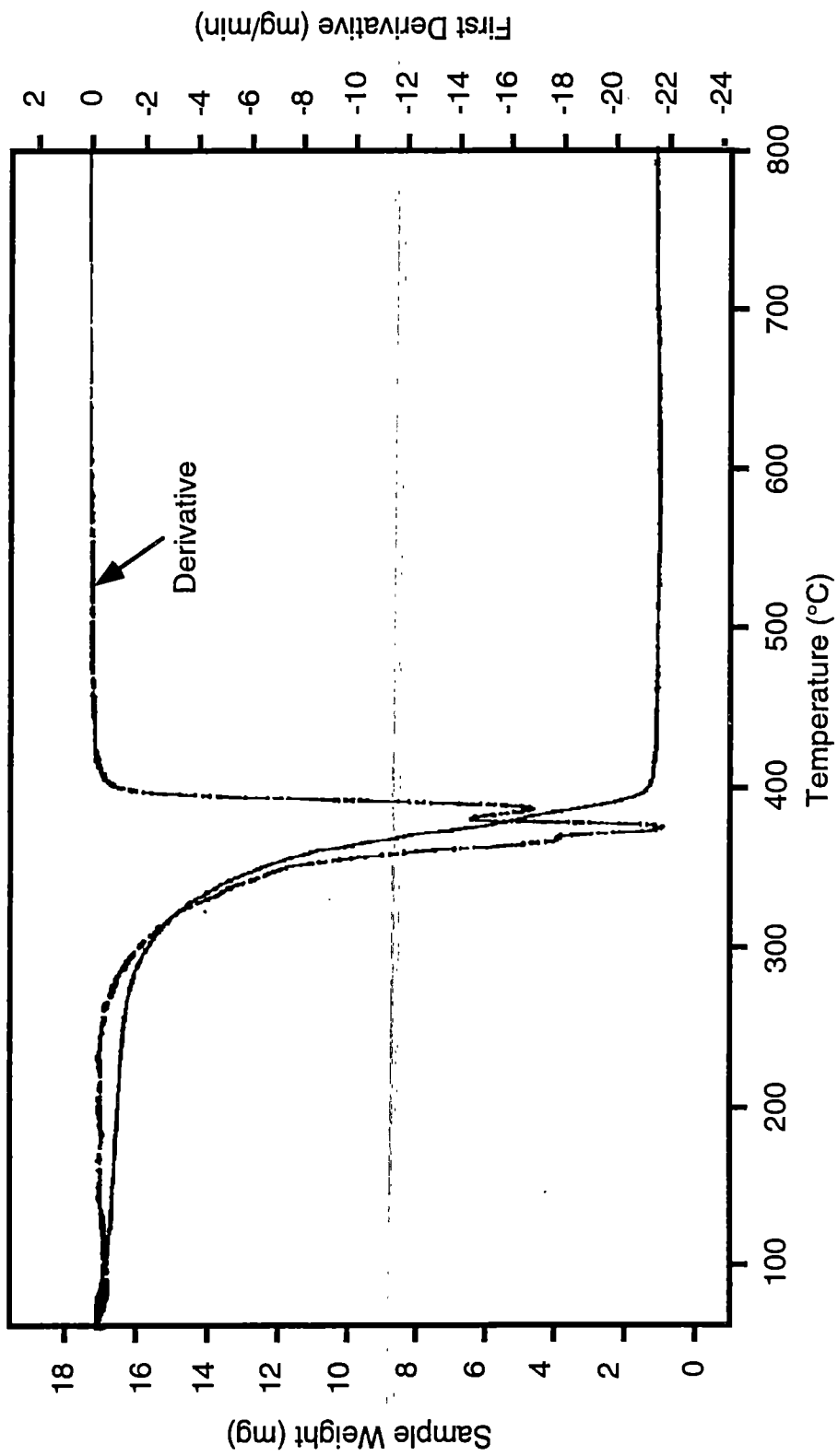


Figure 20. Ba(TMHD)₂ Thermogravimetric Analysis [18].

occur in the (225-300) $^{\circ}$ C temperature range [14, 18] at atmospheric pressure. The absorption observation time for this sample was approximately 8 hours, much longer than the typical thermogravimetric analysis period.

The next Cu(TMHD)₂ absorption experiment used a 0.0008g sample held at a temperature of (92-94) $^{\circ}$ C. The detailed absorption scans of this sample were taken after absorption became stable at this temperature setting. A stabilization time of approximately one hour was required to observe constant vaporization levels at (92-94) $^{\circ}$ C. A continuous scanning speed of 3nm/min was used and the transmission signals averaged over every 0.005nm, as indicated in the procedures section. The chamber pressure was monitored by the capacitance manometer during the this 70min scan. The chamber pressure at the start of the scan was 3.58Torr, and the chamber pressure at the end of the scan was 4.57Torr. Figure 21 illustrates the results this copper (TMHD) absorption I scan and a corresponding baseline I_0 scan at the (92-94) $^{\circ}$ C temperature setting. The I scan is a result of the I_0 output being partially absorbed during transmission through the copper (TMHD) vapor. Therefore, the output of the absorption I scan is lower than the baseline I_0 scan. With the chamber evacuated except for the precursor, this lower output indicates that vaporization of the copper (TMHD) sample had occurred. Figure 22 shows the resulting absorbance measurements of the copper (TMHD) sample as a function of wavelength over the 200nm to 400nm wavelength interval. The absorbance as a function of wavelength was graphically illustrated by utilizing equations 14 and 15. Additionally, detailed absorption scans of the copper (TMHD) sample were taken over the 200nm to 220nm and 220nm to 260nm wavelength intervals using high gain settings (greater photomultiplier tube voltage). This was necessary because of the substantial absorption of the sapphire windows in these wavelength regions. Figure 23 represents the results of the copper (TMHD) absorbance as a function of wavelength over the 200nm to 220nm interval. Similarly, Figure 24 illustrates the Cu(TMHD)₂ absorbance as a function of wavelength over the 220nm to

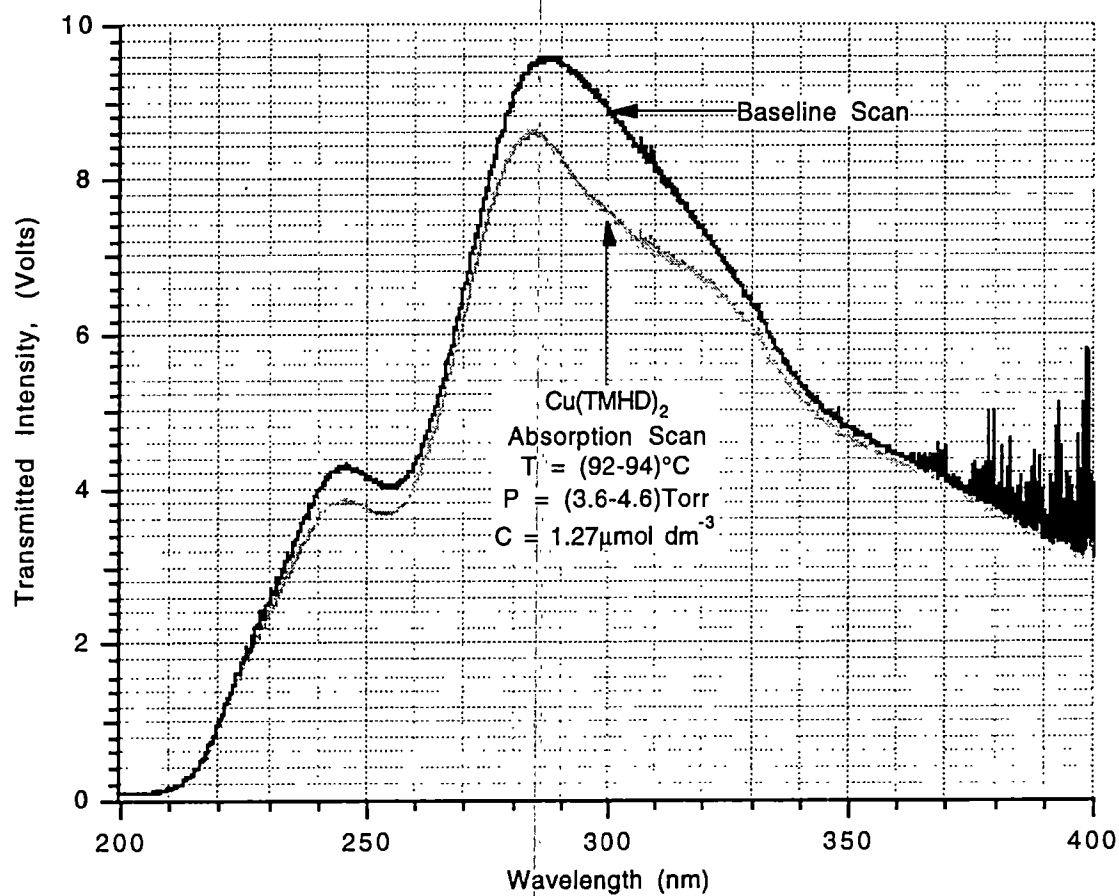


Figure 21. Cu(TMHD)_2 Absorption Scan.

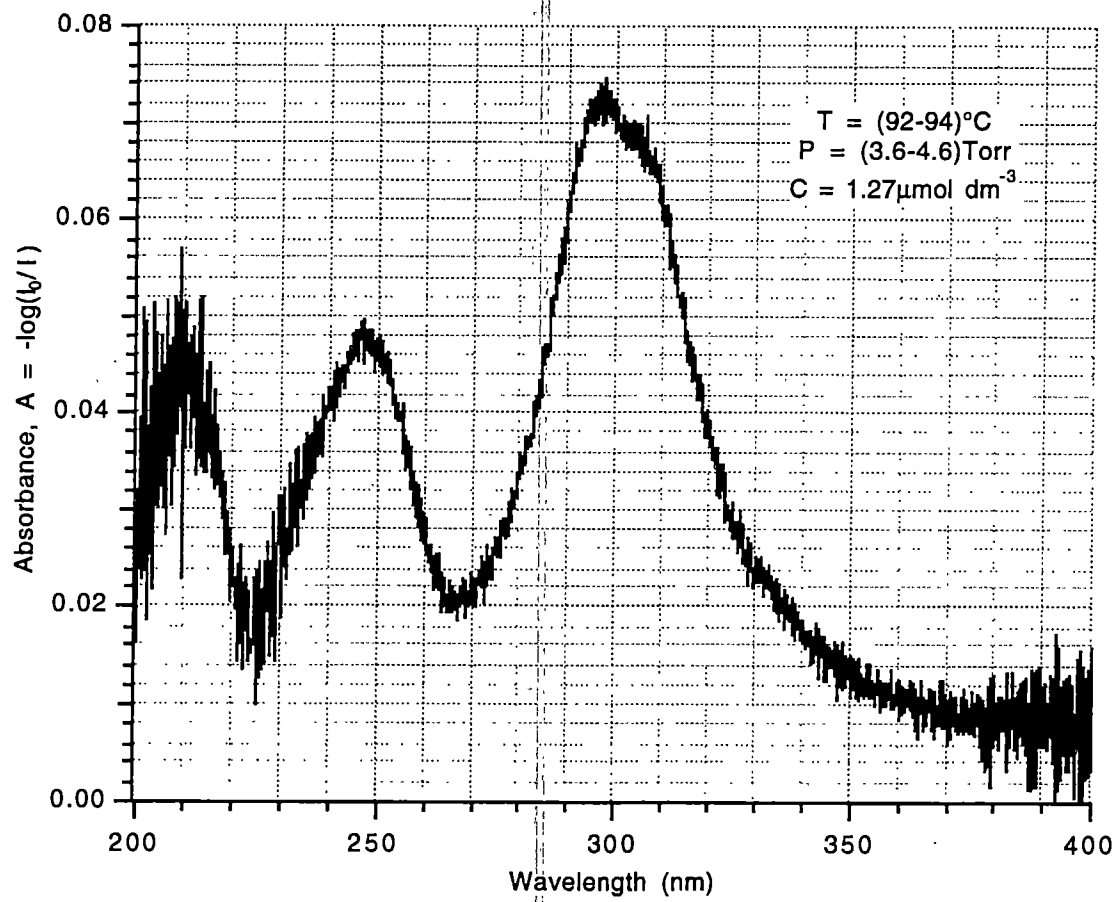


Figure 22. Cu(TMHD)_2 Absorption.

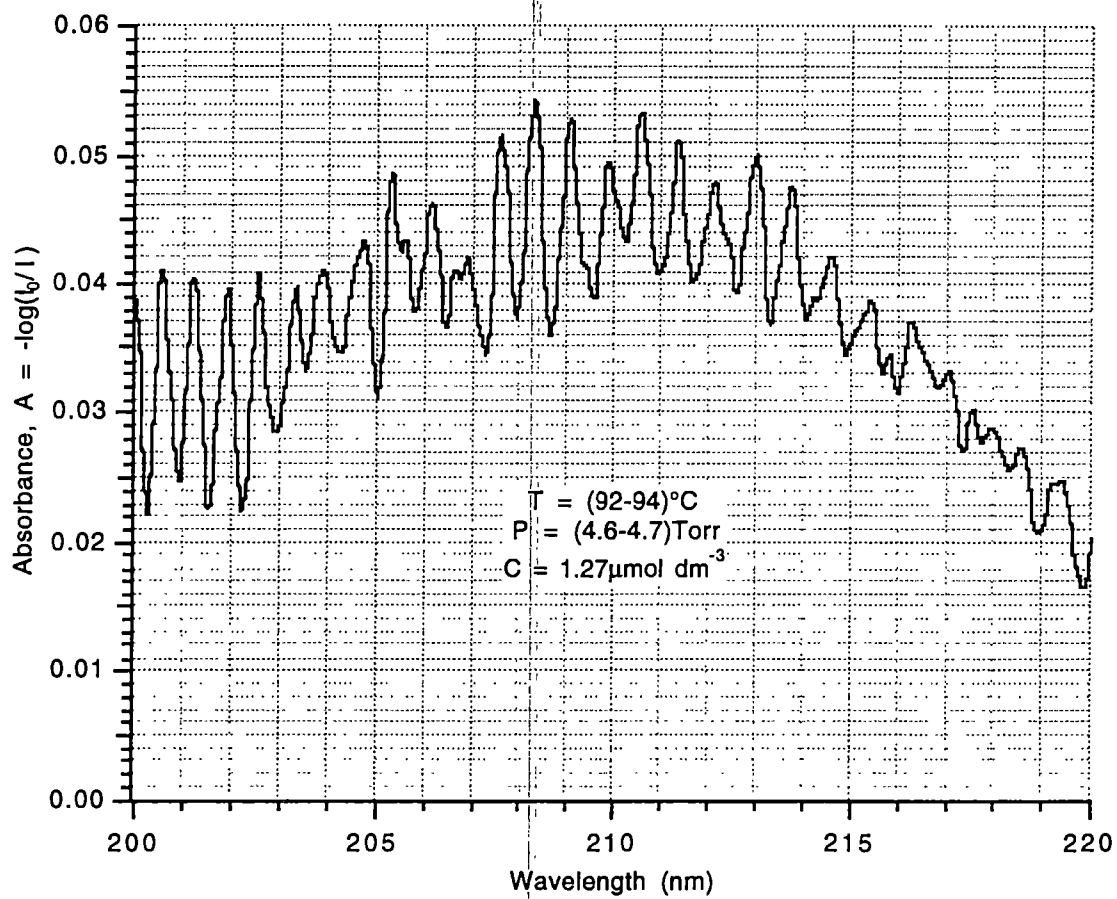


Figure 23. Cu(TMHD)₂ Absorption (200-220)nm Region.

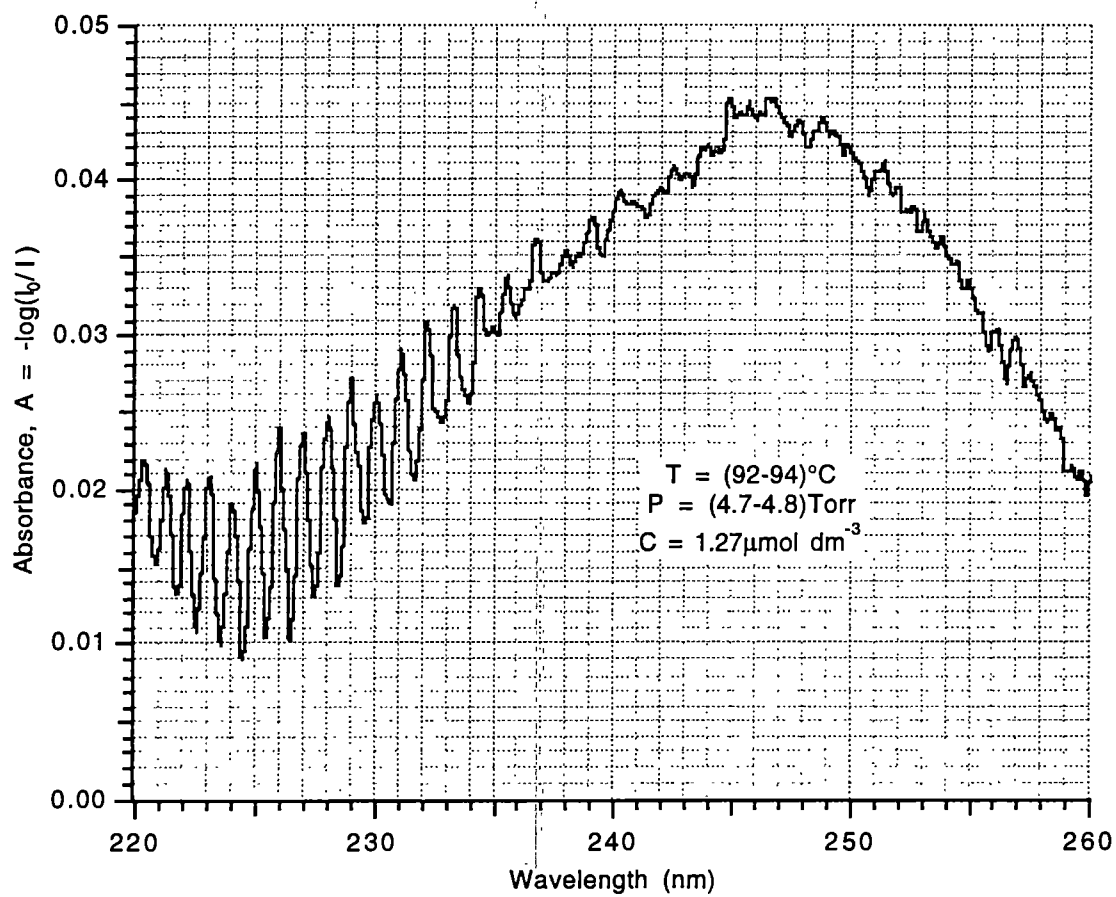


Figure 24. Cu(TMHD)_2 Absorption (220-260)nm Region.

260nm interval. After the transmission scans were completed the oven was cooled and the Cu(TMHD)_2 sample container weighed, indicating no remaining sample. Hence, the sample had completely vaporized during the one hour of heating at constant temperatures of (92-94) $^\circ\text{C}$. The total absorption observation time of this sample was approximately 6 hours.

Y(TMHD)_3 Absorption Experimental Results

The Y(TMHD)_3 precursor was analyzed after the absorption study involving Cu(TMHD)_2 , using the same experimental procedures. An initial Y(TMHD)_3 absorption experiment was conducted using an 0.0008g sample. Rapid scanning in five minute intervals of the 200nm to 400nm wavelength region during the heating process revealed observable vapor absorption of the sample taking place in the (110-120) $^\circ\text{C}$ temperature range, again at considerably lower temperatures than thermogravimetric analysis indicated [14, 18]. Constant increased heating, without holding at one temperature setting for a prolonged period of time, showed absorption levels becoming constant in the (185-195) $^\circ\text{C}$ temperature range. After completion of the transmission scans at 195 $^\circ\text{C}$ and cooling the sample chamber, it was observed that the sample had been completely vaporized. The thermogravimetric analysis data supported near complete vaporization of the yttrium precursor [18], but under vacuum it apparently completely vaporizes. Also, the thermogravimetric analysis data indicated complete vaporization of the yttrium precursor in the (280-300) $^\circ\text{C}$ temperature range [14], a considerably higher temperature than under vacuum. The total absorption observation time of this sample was approximately 8 hours.

An additional yttrium (TMHD) precursor absorption analysis was conducted using a 0.0012g sample in order to obtain a detailed scan at a stable absorption and temperature setting. Rapid absorption scans were taken every five minutes while heating the oven to (123-124) $^\circ\text{C}$. After approximately one hour of maintaining the sample at the (123-124) $^\circ\text{C}$

setting, the absorption levels were stable. A high resolution scan using the standard parameters was taken of the stable Y(TMHD)_3 absorption level at $(123-124)^\circ\text{C}$. The starting and ending chamber pressures during this scan were 4.33Torr and 5.48Torr, respectively. Figure 25 shows the results of the detailed yttrium (TMHD) absorption scan along with a comparable baseline scan. Figure 26 shows the resulting absorbance of the Y(TMHD)_3 sample as a function of wavelength over the 200nm to 400nm interval. After completing the detailed absorption *I* scan, the absorption chamber was cooled. Inspection of the precursor tray following the detailed absorption scan showed that there was no sample remaining. Hence, the sample had completely vaporized during the one hour of heating at a constant temperature of $(123-124)^\circ\text{C}$. The total absorption observation time of this Y(TMHD)_3 sample was approximately 6 hours.

Ba(TMHD)_2 Absorption Experimental Results

The barium (TMHD) precursor was the last precursor examined. The experimental procedures employed in the Cu(TMHD)_2 and Y(TMHD)_3 absorption analyses were utilized. Ba(TMHD)_2 absorption experiments were conducted using a 0.0050g sample. Rapid scanning while the oven temperature was rising revealed that this precursor begins to vaporize in the $(125-135)^\circ\text{C}$ temperature range. This sample was heated to a temperature of $(146-148)^\circ\text{C}$ for an extended period of time. After a one hour observation time utilizing quick scans, the absorption level was observed to be stable. A standard detailed transmission scan was taken of the Ba(TMHD)_2 at a temperature of $(146-148)^\circ\text{C}$. The chamber pressure during this scan was monitored by the capacitance manometer. The initial chamber pressure at the start of the scan was 3.67Torr, and the chamber pressure at the end of the scan was 4.63Torr. Figure 27 illustrates the Ba(TMHD)_2 transmission scan and the baseline scan. Figure 28 shows the Ba(TMHD)_2 absorbance as a function of wavelength over the 200nm to 400nm region.

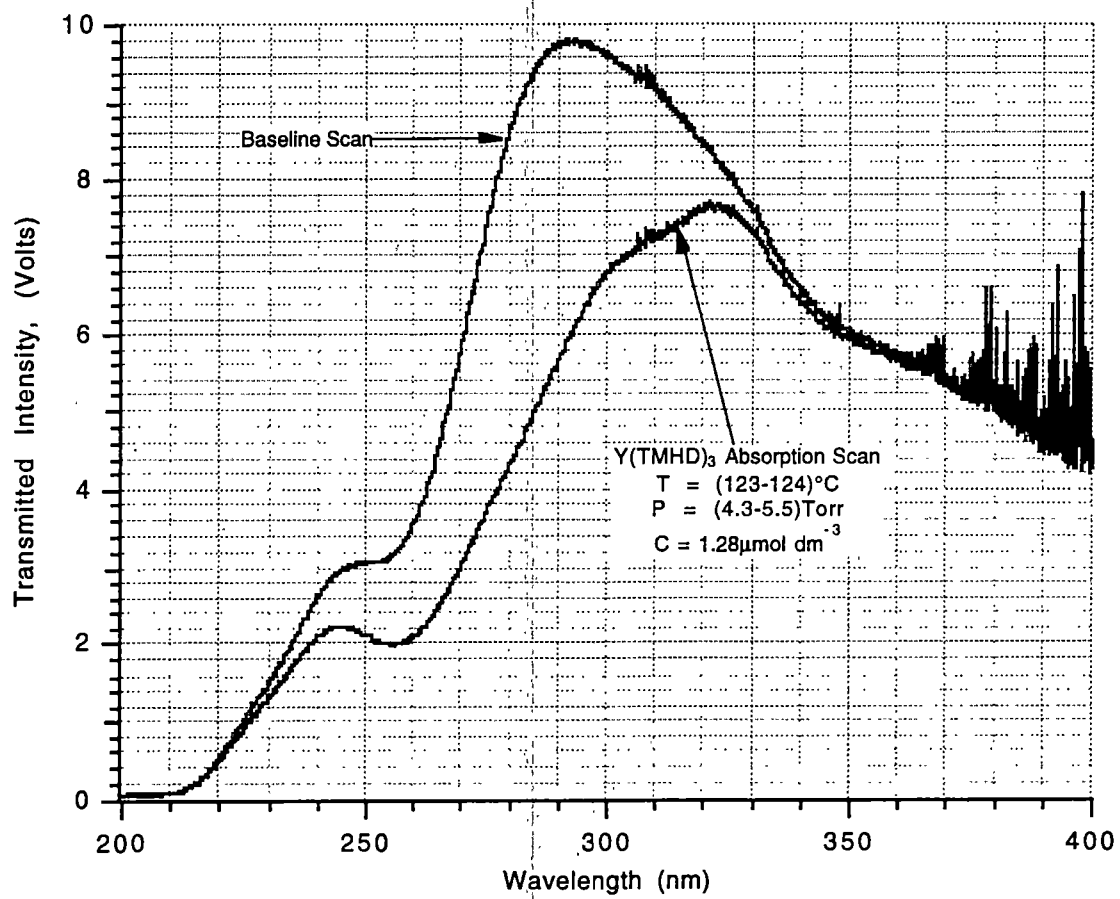


Figure 25. Y(TMHD)₃ Absorption Scan.

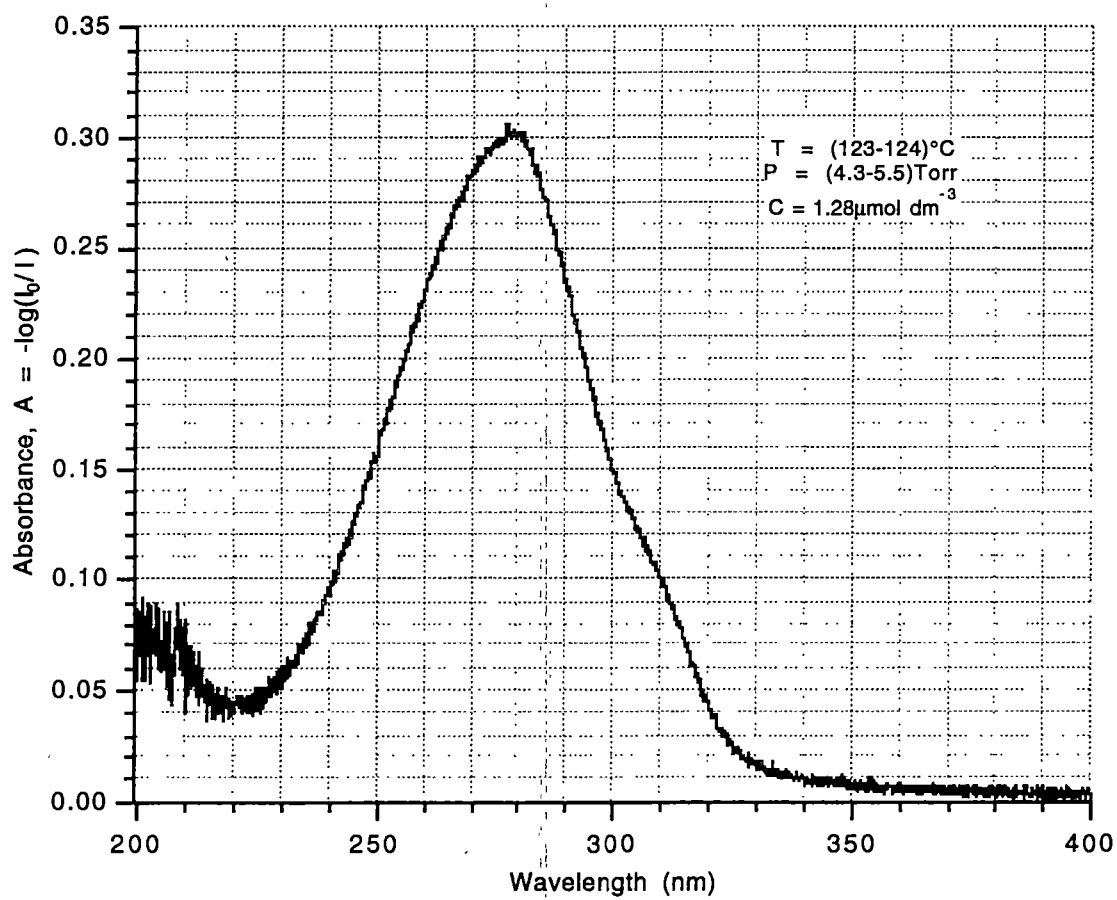


Figure 26. Y(TMHD)₃ Absorption.

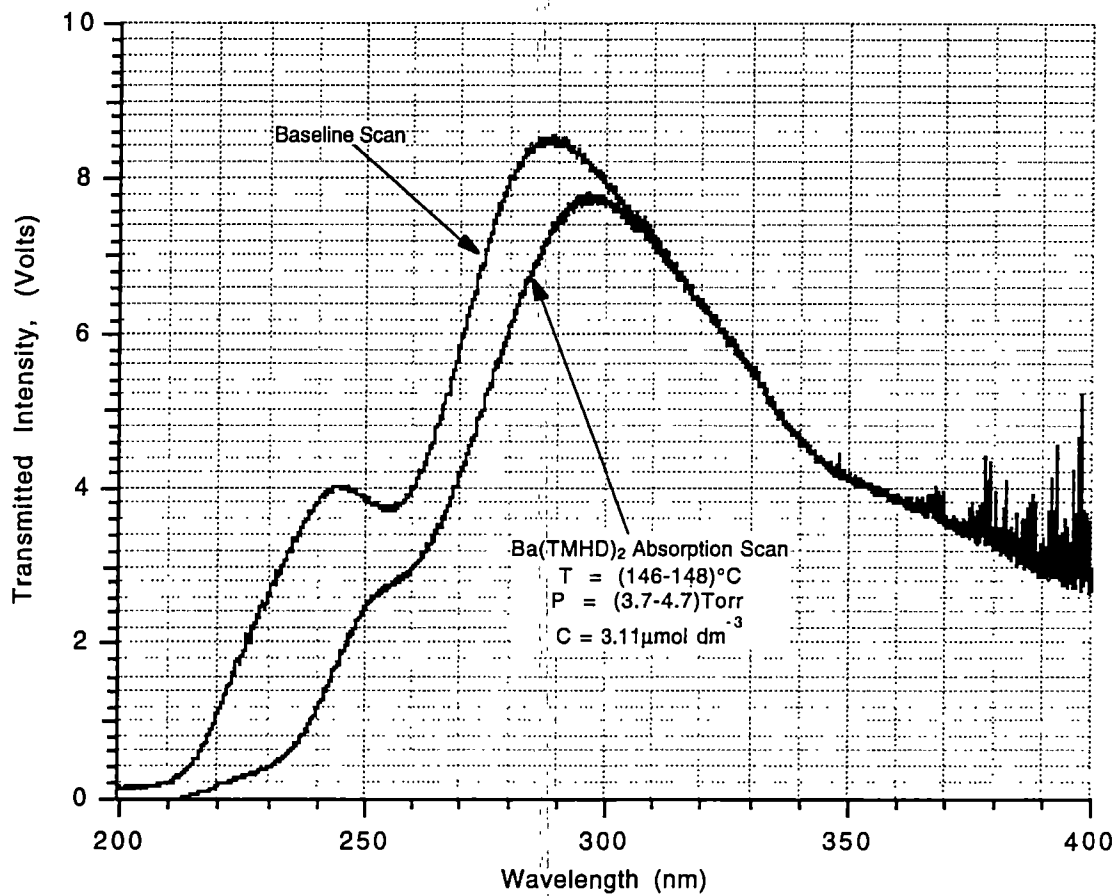


Figure 27. Ba(TMHD)₂ Absorption Scan: Trial 1.

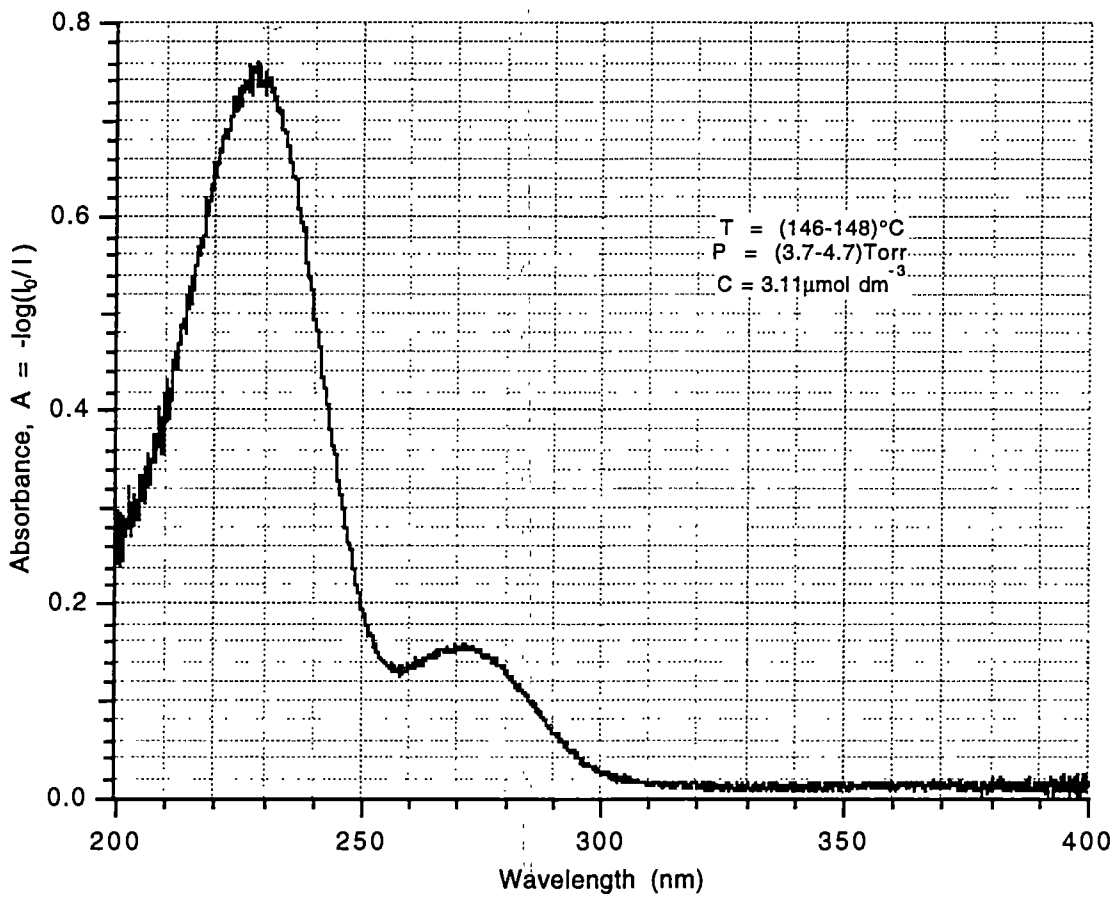


Figure 28. Ba(TMHD)₂ Absorption: Trial 1.

Increasing the oven temperature following the detailed *I* scan, while taking rapid scans, indicated that the Ba(TMHD)₂ continues to vaporize as the temperature is raised. The Ba(TMHD)₂ sample exhibited stable absorption levels only when the temperature was raised to 300°C, the high temperature limit of the oven. However, as this was the upper temperature limit, it was unclear if the barium (TMHD) was completely vaporized. After completing the absorption scans, inspection of the precursor tray showed that the sample had only been partially vaporized. The post-heating sample weight was 0.0027g. Therefore, 0.0023g of the original 0.0050g Ba(TMHD)₂ sample had been vaporized. The partial vaporization of the barium (TMHD) sample was supported by the thermogravimetric analysis [18]. Reference [14] indicated that the barium precursor only has 73% sample vaporization at 400°C and never completely vaporizes. The total absorption observation time of this sample was 4 hours. Figure 28 shows a large absorption peak in the (200-250)nm region that is not present in the absorption scans found in the literature (see Figure 3). Therefore, an additional Ba(TMHD)₂ absorption experiment was conducted to rule out degradation of the Ba(TMHD)₂ that might have occurred if the sample chamber leaked.

An experiment was devised to check for suspected contamination due to air leakage into the absorption cell. Repeating the scans in an argon environment at initially slightly greater than one atmosphere chamber pressure would produce outgasing instead of contamination if the chamber leaked, so if the additional absorption peak in Figure 28 resulted from contamination it should not appear in these scans. A 0.0045g Ba(TMHD)₂ sample was analyzed in this experiment. After a one hour observation time to reach stable absorption conditions, a standard high resolution scan was conducted at a temperature of (157-159)°C. The higher temperature was necessary due to the pressurized argon environment. The chamber pressure during this scan was approximately 760Torr. Figure 29 illustrates the results of the positive chamber pressure Ba(TMHD)₂ transmission scan

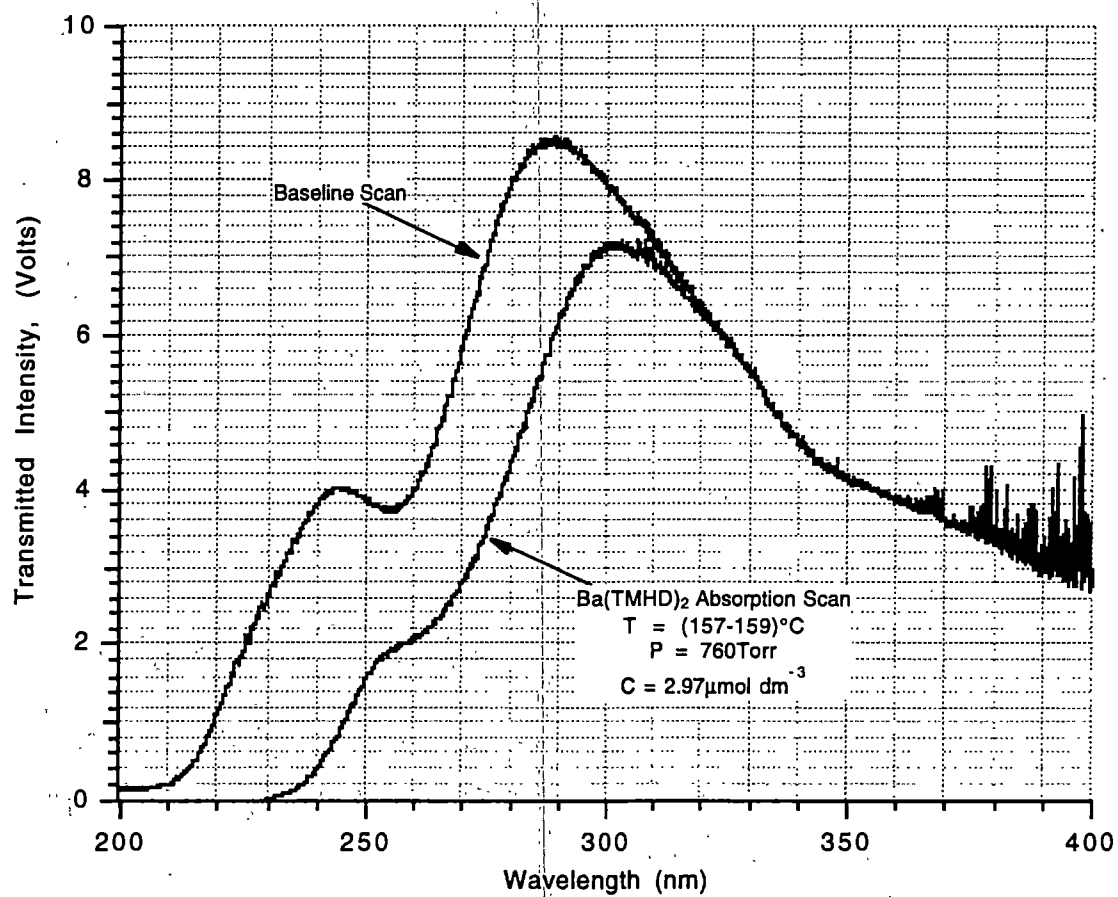


Figure 29. Ba(TMHD)₂ Absorption Scan: Trial 2.

along with the baseline scan. Figure 30 shows the resulting absorbance of the $\text{Ba}(\text{TMHD})_2$ sample as a function of wavelength over the 200nm to 400nm interval and confirms the large absorption peak in the (200-250)nm wavelength region as reported in Figure 28. Therefore, the large absorption peak in the (200-250)nm wavelength region was not a result of an inward leak contaminating the $\text{Ba}(\text{TMHD})_2$. Tests were also run on the sapphire window transmission at temperatures of -7°C , -6°C , $+5^\circ\text{C}$, and $+7^\circ\text{C}$ from the scan temperature of 147°C . As shown in Figure 31, only small random absorbance is indicated, which is insufficient to explain the new $\text{Ba}(\text{TMHD})_2$ peak. The discrepancy in the absorbance curves presented in Figures 3, 28, and 30 could be due to differences in the barium precursor material analyzed. The $\text{Ba}(\text{TMHD})_2$ materials analyzed in this study were supplied by ATM and could have degraded while in the UTSI glove box storage. The $\text{Ba}(\text{DPM})_2$ materials analyzed in the study presented in Figure 3 were supplied by Toso Akuzo Company [15].

After, completion of the high resolution absorption scan at $(157-159)^\circ\text{C}$, the sample chamber was cooled. Inspection of the precursor sample tray revealed that the sample had again only partially vaporized. The post-test sample weight was 0.0023g. Therefore, 0.0022g of the original 0.0045g sample had been vaporized during the one hour of heating at stable temperatures of $(157-159)^\circ\text{C}$. The total absorption observation time was approximately 4 hours.

Analysis of Results

A comparison of the experimental absorption peak wavelengths with the absorption peak wavelengths found in the literature (see Figure 3) are presented in Table 3. Table 3 indicates that a less than 5% difference exists between the experimental and reference results of the absorption peak wavelengths of the barium, copper, and yttrium precursors, except for the new barium peak in the (200-250)nm region.

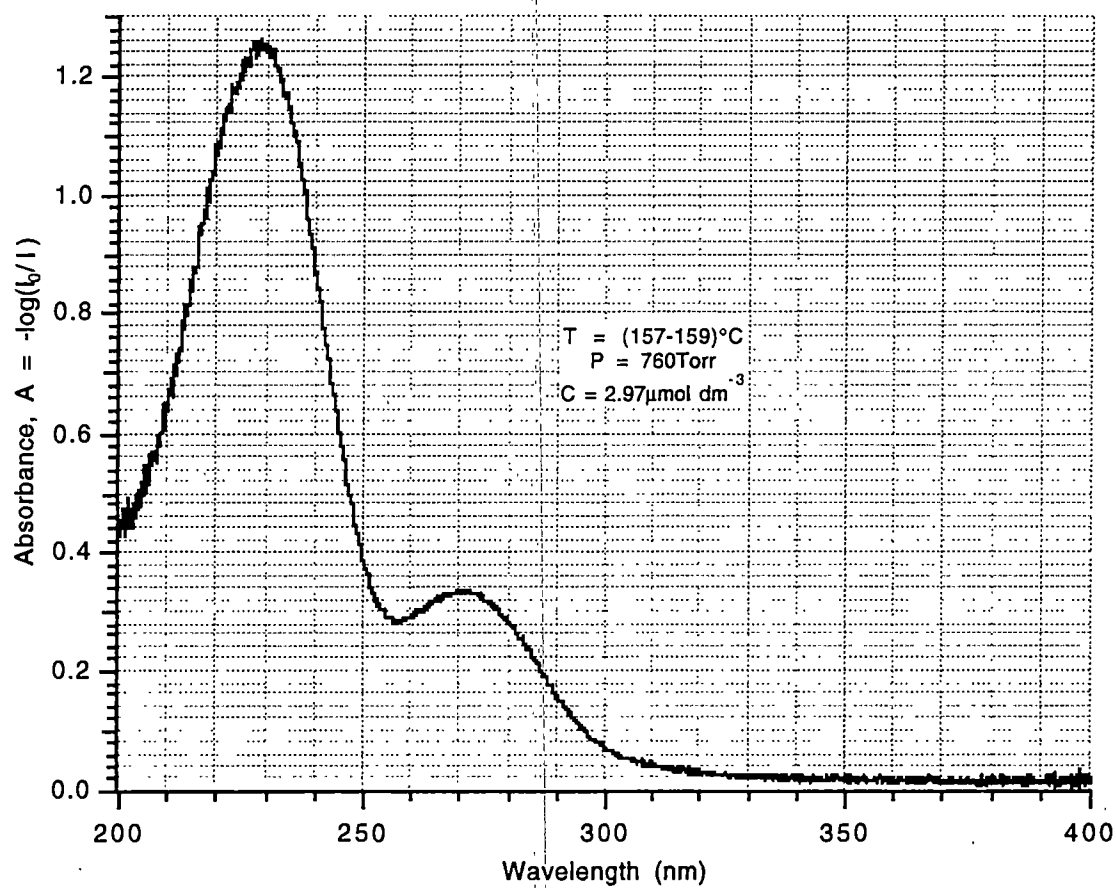


Figure 30. Ba(TMHD)₂ Absorption: Trial 2.

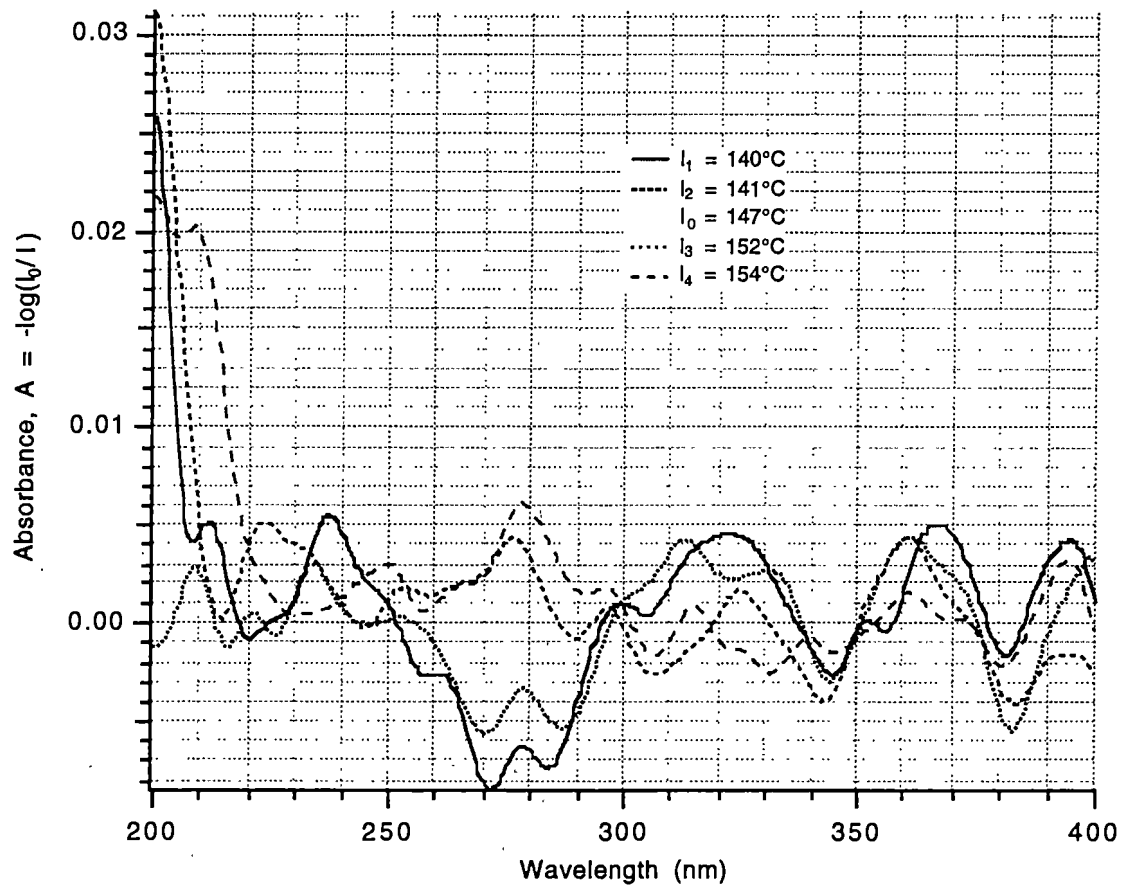


Figure 31. Transmission Check of Sapphire Windows.

Table 3. Comparison of Measured Absorption Peak Wavelengths with Reference [15].

Precursor Sample Type	Experimental Absorption Figure No.	Experimental Absorption Peak Wavelength (nm)	Reference (Figure 3) Absorption Peak Wavelength (nm)	Percent Difference ((reference - measured)/reference)x100 (%)
Cu(TMHD) ₂	22	247	249 (250)	0.803 (1.20)
		298	298 (297)	0 (0.337)
Cu(TMHD) ₂	23	208.25	202 (201)	3.09 (3.61)
Cu(TMHD) ₂	24	248	249 (250)	0.402 (0.80)
Y(TMHD) ₃	26	280	280	0
Ba(TMHD) ₂	28	228	—	—
		273	274	0.365
Ba(TMHD) ₂	30	230	—	—
		272	274	0.730

Utilizing the Beer's law form in equation 13, $A = abc = \log(I_0/I)$, and the results of the precursor absorption experiments, the extinction coefficient (absorptivity) a could be calculated for each precursor at each absorption peak. Solving equation 13 for a , yields

$$a = A/bC \quad (20)$$

Equation 20 was employed to determine the gas phase Cu(TMHD)_2 , Y(TMHD)_3 , and Ba(TMHD)_2 extinction coefficients from the precursor high resolution absorption scans. The dimensionless absorbance A values for these calculations were determined graphically from the experimental precursor absorption results. The experimental pathlength b was the absorption chamber flange-to-flange length measurement, measured to be 50.8cm. The molar vapor concentration of each precursor sample was determined using equation 16. Therefore, the extinction coefficient values are reported in units of $\mu\text{mol dm}^{-3}$. The results of these calculations are presented in Table 4. As mentioned previously, the concentration uncertainties are significant, so these absorptivity values also will have significant uncertainties.

A sensitivity calculation was also made for the barium, yttrium, and copper (TMHD) precursors at the experimentally determined absorption peak wavelengths and the corresponding absorbance A values resulting from the detailed absorption I scans. This calculation was made by assuming a constant b and calculating the precursor concentration C necessary to give a 1% absorbance A . Table 5 shows the results of the sensitivity calculations for the copper, yttrium, and barium (TMHD) precursors. The concentration values of the samples are in $\mu\text{mol dm}^{-3}$ units. These concentration values are rather high for the small samples used in the experimentation. Since the sample sizes used and the vapor concentrations of the precursors were very small, then Table 5 indicates that high sensitivity monitoring of the precursors by absorption spectroscopy is attainable. Hence, this high sensitivity result implies that absorption spectroscopy is capable of monitoring the vapor concentrations of very small precursor concentrations.

Table 4. Precursor Extinction Coefficient Calculations.

Precursor Sample	Experimental Absorption Figure No.	Experimental Absorption Peak Wavelength (nm)	Experimental Graphical Absorbance, A Value $A = -\log(I_0/I)$	Initial Sample Mass (g)	Post-Scan Sample Mass (g)	Precursor Sample Vapor Mass, <i>m</i> (g)	Precursor Molecular Weight, <i>M</i> (g/mol)	Precursor Vapor Concentration, $C = m/(MV)$ <i>V</i> = 1.47L ($\mu\text{mol dm}^{-3}$)	Experimental Precursor Extinction Coefficient, $a = A/bC$ ($\text{mol dm}^{-3}\text{-}^{-1}\text{cm}^{-1}$) <i>b</i> = 50.8cm	Molar Extinction Coefficient ($10^3\text{mol}^{-1}\text{cm}^{-1}$) Figure 3 Reference [15]
Cu(TMHD) ₂	22	247	0.050	0.0008	0	0.0008	430.09	1.27	780	1.5
Cu(TMHD) ₂	22	298	0.074	0.0008	0	0.0008	430.09	1.27	1100	1.9
Cu(TMHD) ₂	23	208.25	0.054	0.0008	0	0.0008	430.09	1.27	840	1.1
Cu(TMHD) ₂	24	248	0.045	0.0008	0	0.0008	430.09	1.27	700	1.5
Y(TMHD) ₂	26	280	0.300	0.0012	0	0.0012	638.73	1.28	4600	3.0
Ba(TMHD) ₂	30	230	1.250	0.0045	0.0023	0.0022	503.89	2.97	8300	-----
Ba(TMHD) ₂	30	272	0.340	0.0045	0.0023	0.0022	503.89	2.97	2300	2.2

Table 5. Sensitivities of Cu(TMHD)₂, Y(TMHD)₃, and Ba(TMHD)₂.

Precursor Sample	Experimental Absorption Figure No.	Experimental Absorption Peak Wavelength (nm)	Experimental Graphical Absorbance, A Value $A = -\log(I_0/I)$	1% Absorbance ($A \times 0.01$)	Concentration, $C = (1\% \cdot A)/b$ $b = 50.8 \text{ cm}$ ($\mu\text{mol dm}^{-3}$)
Cu(TMHD) ₂	22	247	0.050	0.00050	9.8
Cu(TMHD) ₂	22	298	0.074	0.00074	15
Cu(TMHD) ₂	23	208.25	0.054	0.00054	11
Cu(TMHD) ₂	24	248	0.045	0.00045	8.9
Y(TMHD) ₃	26	280	0.300	0.00300	59
Ba(TMHD) ₂	28	228	0.760	0.00760	150
Ba(TMHD) ₂	28	273	0.160	0.00160	31
Ba(TMHD) ₂	30	230	1.250	0.01250	250
Ba(TMHD) ₂	30	272	0.340	0.00340	67

An ideal gas law calculation, solving for the vapor pressure P , was made for each of the detailed transmission scans. This calculation was made utilizing the following form of the ideal gas law

$$PV = nRT \quad (21)$$

where V was the measured chamber volume of 1.47L, n was the number of moles in the precursor vapor concentration, R was the gas constant, 62.364((Torr L)/(K mol)), and T was the constant temperature upper bound. Table 6 presents the results of these calculations. The vapor pressures determined through equation 21 are lower than the pressures indicated on the absorption figures due to the slight chamber leak.

Lastly, Figure 32 shows the baseline scans at the indicated temperatures for the detailed precursor transmission scans.

Table 6. Precursor Vapor Pressure Calculations.

Precursor Sample	Number of Moles, n (mol)	Temperature, T Upper Bound (K)	Vapor Pressure, P $P = (nRT)/V$ $R = 62.364((\text{Torr L})/(\text{K mol}))$ $V = 1.47\text{L}$ (Torr)
Cu(TMHD) ₂	1.87×10^{-6}	367.2	0.03
Y(TMHD) ₃	1.88×10^{-6}	397.2	0.03
Ba(TMHD) ₂	4.37×10^{-6}	421.2	0.08

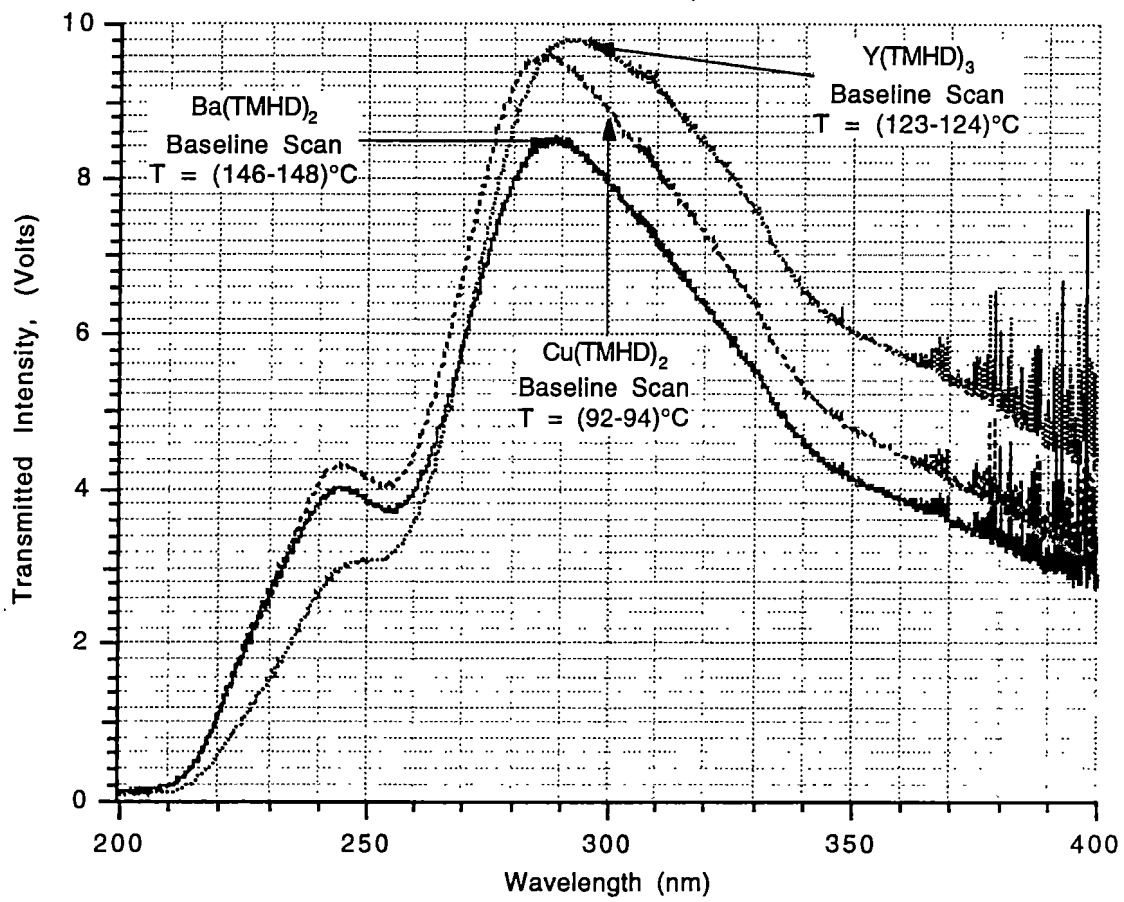


Figure 32. Detailed Precursor Baseline Scans.

CHAPTER V

CONCLUSIONS AND RECOMMENDATIONS

Experimental results from this research effort indicate that absorption spectroscopy is a feasible diagnostic for monitoring the YBCO precursor vapor concentrations during MOCVD processing. The results show that absorption spectroscopy yields high sensitivity which enables the monitoring of the vapor concentrations of very small concentrations of the Cu, Y, and Ba MOCVD precursors. Results of the absorption experiments indicate that prolonged monitoring of precursor vapor concentrations is attainable. Additionally, the experimental results provide critical information relevant to temperature ranges at which the precursors experience initial vaporization under MOCVD vacuum conditions. All of the (TMHD) precursors analyzed showed that stable absorption levels were observable for extended periods of time (1-2 hours). The results of the Cu(TMHD)_2 , Y(TMHD)_3 , and Ba(TMHD)_2 experiments show that these precursors begin to vaporize between 90°C and 135°C , temperatures considerably lower than atmospheric thermogravimetric analysis indicates [14, 18]. Additionally, the Cu(TMHD)_2 and Y(TMHD)_3 precursors are completely vaporized after heating periods of about one hour at temperatures of 90°C to 125°C . The Ba(TMHD)_2 experiments indicate that this precursor experiences about 50% vaporization after extended heating periods of temperatures between 100°C and 300°C .

The results of the Cu(TMHD)_2 absorption analyses indicate that this precursor begins changing to the vapor state in the $(90-95)^\circ\text{C}$ temperature range and is completely vaporized between 145°C and 155°C using rapid heating. Stable absorption conditions for extended periods of time, one to two hours, permitted detailed absorption scans. All absorption experiments involving the Cu(TMHD)_2 precursor resulted in total vaporization of the sample in a less than 1 Torr vacuum after about an hour at a constant temperature of $(90-95)^\circ\text{C}$. Additionally, the absorbance peak wavelengths identified in Figures 22, 23,

and 24 are in good agreement with the reference absorbance peak wavelengths for Cu(TMHD)_2 solved in hexane as presented in Figure 3.

The results of the Y(TMHD)_3 absorption analyses show that this precursor in a vacuum experiences initial vaporization in the (110-120) $^\circ\text{C}$ temperature interval and is completely vaporized between 185 $^\circ\text{C}$ and 195 $^\circ\text{C}$ using rapid heating. Stable absorption conditions for extended periods of time were also attainable for this precursor. Similar to the Cu(TMHD)_2 samples, all of the absorption experiments involving the Y(TMHD)_3 precursor in a less than 5Torr vacuum resulted in total vaporization of the sample after about an hour at constant temperatures as low as (120-125) $^\circ\text{C}$. Likewise, the absorbance peak wavelength identified in Figure 26 is identical to the reference absorbance peak wavelength presented in Figure 3.

Results of the Ba(TMHD)_2 absorption tests indicate that this precursor at vacuum experiences initial vaporization in the (125-135) $^\circ\text{C}$ temperature range. However, all absorption analyses involving this precursor reveal that it only partially vaporizes at temperatures up to 300 $^\circ\text{C}$. Approximately 50% of the Ba(TMHD)_2 precursor pre-heat mass was vaporized. A large absorption peak in the (200-250)nm region identified in Figure 28 and Figure 30 is not present in the reference Ba(TMHD)_2 scans presented in Figure 3. This could be due to differences in the precursor materials used in the experimentation or the samples themselves being contaminated before this research effort was conducted.

Recommendations pertaining to the design and development of in situ absorption spectroscopy diagnostics to monitor YBCO fabrication by MOCVD are a result of this research effort. The 50.8cm pathlength of the absorption chamber resulted in high absorption of the precursor samples. Since these precursor materials are so absorptive in the UV wavelength region, it is clear that the method would be very sensitive and needs a short pathlength.

Appropriate future work on this research effort includes covering other wavelength intervals. Also, utilizing better optical mounting arrangements would eliminate the constant alignment requirements. The analysis of precursor samples produced by different manufacturers would allow a more thorough investigation of the precursor vapor properties, particularly for Ba(TMHD)_2 . Further absorption experiments with the Ba(TMHD)_2 precursor in the (200-250)nm wavelength region are needed to determine the validity of the observed (200-250)nm peak shown in Figure 28 and Figure 30. Scans of a different Ba(TMHD)_2 sample are particularly recommended. Likewise, conducting absorption analyses of a mixed sample composed of all three precursors would determine if the absorption spectra of the precursors are distinguishable. This would allow evaluation of absorption spectroscopy as a monitor of MOCVD chamber concentrations of all three precursors simultaneously. Finally, more accurate concentration measurements are needed so accurate molar absorptivities can be determined.

REFERENCES

REFERENCES

- [1] Owens, F.J. and Poole, C.P., *The New Superconductors*, Plenum Press, New York, 1996.
- [2] "The History of Superconductors," Colorador Superconductor, Inc., Internet: <http://www2.csn.net/~donsher/history.html>, 1997.
- [3] "Superconductivity: History," U.S. Department of Energy, Internet: <http://www.eren.doe.gov/superconductivity/history.html>, 1999.
- [4] Yam, Philip., "Trends in Superconductivity: Current Events," *Scientific American*, **269** (6), pp. 84-93, December 1993.
- [5] "Evaluation of Methods for Application of Epitaxial Buffer and Superconductor Layers," DE-AC22-95PC95231, UTSI, June 1997.
- [6] Rappoli, B.J. and DeSisto, W.J., "Gas Phase Ultraviolet Spectroscopy of High-Temperature Superconductor Precursors for Chemical Vapor Deposition Processing," *Appl. Phys. Lett.*, **68** (19), pp. 2726-2728, May 1996.
- [7] Singh, R., Sinha, S. Hsu, N.J., Chou, P., Singh, R.K., and Narayan, J., "Superconducting Thin Films of Y-Ba-Cu-O Prepared by Metal Organic Chemical Vapor Deposition," *J. Appl. Phys.* **67** (3), pp. 1562-1565, February, 1990.
- [8] Kaloyeros, A.E., Feng, A., Jahn, E., and Brooks, K.C., "Metal-Organic Chemical Vapor Deposition (MOCVD) of High Temperature Superconductors with Enhanced Critical Current," *American Institute of Physics*, pp. 470-477, 1991.
- [9] Norris, P. and Zhao, J., "Progress in the Growth of $\text{YBa}_2\text{Cu}_3\text{O}_{7-x}$ Thin Films by MOCVD and Prospects for Large Area, Low Temperature Deposition," *American Institute of Physics*, pp. 63-72, 1992.
- [10] Mavrodineanu, R. and Boiteux, H., **Flame Spectroscopy**, John Wiley & Sons, Inc., New York, 1965.
- [11] Ramçrez-Muñoz, J., **Atomic-Absorption Spectroscopy**, Elsevier Publishing Company, Amersterdam, 1968.
- [12] UV Spectrometry Group, **UV Spectroscopy Techniques, Instrumentation, Data Handling**, Chapman & Hall, London, 1993.
- [13] Bauman, R.P., **Absorption Spectroscopy**, John Wiley & Sons, Inc., New York, 1962.
- [14] Harima, H., Ohnishi, H., Hanaoka, K., Tachibana, K., Kobayashi, M., and Hoshinouchi, S., "Spectroscopic Study on a Discharge Plasma of MOCVD Source Gases for High- T_c Superconducting Films," *Japanese Journal of Applied Physics*, **29** (10), pp. 1932-1938, October 1990.

- [15] Harima, H., Ohnishi, H., Hanaoka, K., Tachibana, K., and Goto, Y., "An IR Study on the Stability of Y(DPM)_3 , Ba(DPM)_2 and Cu(DPM)_2 for UV Irradiation," *Japanese Journal of Applied Physics*, **30** (9A), pp. 1946-1955, September 1991.
- [16] Hanaoka, K., Ohnishi, H., Harima, H., and Tachiban, K., "In Situ Infrared Absorption Spectroscopy on the Thermal Decomposition Process of MOCVD Source Gases for YBCO Thin Films," *Physica C*, **190**, pp. 145-147, 1991.
- [17] Fackler, J., Cotton, F., and Barnum, D., "Electronic Spectra of β -Diketone Complexes. III. α -Substituted β -Diketone Complexes of Copper(II)," *Inorganic Chemistry*, Vol. 2, No. 1, pp. 97-101, February 1963.
- [18] Bridges, A., Personal communication, UTSI, 1998.

VITA

Matthew Edward Thomas was born in Dayton, Ohio on March 31, 1975. He graduated from Fleming County High School in Flemingsburg, Kentucky in May of 1993. Matthew entered Morehead State University in Morehead, Kentucky in the fall of 1993. While a student at Morehead State University, Matthew was a member of the Morehead State cross country and track teams, including the 1995 Ohio Valley Conference cross country championship team. In May of 1997, he received a Bachelor of Science degree with a double major in Physics and Mathematics. He began his graduate studies at the University of Tennessee Space Institute in August of 1997 toward the degree of Master of Science in Engineering Science. Matthew officially received this degree in May of 1999.